Pergamon

Journal of Structural Geology, Vol. 17, No. 10, pp. 1425 to 1443, 1995

0191-8141/95 $9.50+0.00

0191-8141(95)00038-0

Deformation-induced clinopyroxene fabrics from eclogites

GASTON GODARD and HERMAN L. M. van ROERMUND*

CNRS-URA 736, Laboratoire de Pétrologie Métamorphique, Université Paris 7, 4 place Jussieu, 75252 Paris Cédex 05, France

(*Received* 17 *June* 1994; *accepted in revised form* 20 *March* 1995)

Abstract—Clinopyroxene (omphacite) microfabric studies in eclogites are useful in characterizing the deformation that has affected deeper parts of subduction zones. We present the microfabrics and TEM structures of four samples representative of the various deformation types known in eclogites. The [001] axis tends to be parallel to the lineation while the (010) plane is close to the foliation, but these general features undergo strong variations in relation to the shape fabric: in strongly-lineated samples, [010] tends to be spread out in a great circle normal to the lineation, whereas [001] is dispersed in the foliation in the case of strongly-foliated samples. The slip systems identified by TEM are [001](100), [001]{110} and 1/2<110>{$\bar{1}$10}. Operation of dislocation creep is testified by the presence of dislocations and dislocation walls, but this process alone cannot explain all the observed features, particularly some aspects of the crystallographic preferred orientation, hence other deformation mechanisms must be involved. These may be dynamic migration recrystallization by grain boundary migration, as well as mass transfer processes. This study illustrates that not every crystallographic mineral preferred orientation can be explained by dislocation glide and/or twinning processes alone. In addition, it also demonstrates that eclogite microfabrics can be used to unravel deformation parameters in subduction and/or collision zones.

INTRODUCTION

Eclogites have a crucial role in the construction of geodynamic models that are concerned with convergent plate margins. They offer the possibility of constructing *PTt* trajectories and thus constrain the evolution of an orogenic belt. However, in addition to usual variables like pressure (*P*), temperature (*T*) and fluid composition, other parameters defining the kinematic framework (stress magnitude, strain rate, finite strain ellipsoid) ought also to be defined in order to constrain such evolutionary schemes. Eclogites relatively unaffected by retrogressive metamorphism, for example, can provide valuable information on the deformation parameters that have been operative in deeper parts of subduction and/or collision zones. In addition, a better knowledge of the eclogite fabrics is also important for a sound interpretation of seismic reflection data from deeper levels of subduction zones.

The deformation parameters can be determined using microfabric analysis. Such microfabric studies have thus far principally been carried out on monomineralic aggregates such as metals, ice, quartzites, marbles and peridotites. The rheological behaviour of these aggregates is controlled by the properties of only one mineral and is thus easy to model. In contrast, systematic microfabric studies of eclogites are still lacking, except for a few early studies (e.g. Engels 1972, Helmstaedt *et al.*, 1972). This is mainly due to the following reasons:

(a) Eclogites are not monomineralic rocks. They are made of garnet (about 30–45 vol.%) and omphacite (60–45 vol.%), the latter being a clinopyroxene (cpx) solid solution of augite, jadeite and aegirine. Nevertheless, earlier studies have already indicated that, during plastic deformation, garnet essentially acts as a rigid body (Godard 1981, Van Roermund & Boland 1981, Van Roermund 1983, Godard 1988, Buatier *et al.*, 1991), except at very high *T* (Smith & Wenk 1980, Van Roermund 1989, 1992, Ando *et al.*, 1993). The rheological behaviour of eclogites is thus largely controlled by omphacite.

(b) Plastic deformation mechanisms operative in cpx are not well understood and, therefore, attempts to interpret strain-induced cpx fabrics have thus far not been very successful (Mercier 1985, Godard 1988, Mainprice & Nicolas 1989). However, numerous recent experimental deformation studies assisted by TEM observations may contribute to overcome this problem.

(c) The classical data acquisition method using universal stage techniques is time-consuming and not very accurate. Because cpx is monoclinic, measurements of cleavage orientation are needed but, unfortunately, cleavage in omphacite is weak and hard to observe. The recently developed technique of electron channelling (Lloyd 1987, Lloyd *et al.*, 1987), will in future improve the quality of the data and reduce the acquisition time.

Before applying systematic microfabric studies to omphacite in eclogites, it is necessary to identify, in nature and in experiments, the operating deformation mechanisms and to characterize the strain-induced omphacite microfabrics in relation to some of the deformation parameters (e.g. strain type, strain rate, stress magnitude). This is the subject of the present article.

First, we present the microfabric analyses of four eclogite samples which were selected as being represen-

*Present address: Department of Geology, Institute of Earth Sciences, Utrecht University, P.O. Box 80.021, 3508 TA Utrecht, The Netherlands.

Table 1. Omphacite compositions and PT estimates

Sample	Gal		Seve78		G10		C22 (matrix)		C22 (ins. Ga)	
Number	20		33		27		42		75	
	Average	σ	Average	σ	Average	σ	Average	σ	Average	σ
Si	1.967	0.015	1.979	0.009	1.958	0.011	1.983	0.008	1.986	0.012
Aliv	0.033	0.015	0.021	0.009	0.042	0.011	0.017	0.008	0.014	0.011
Alvi	0.375	0.011	0.461	0.012	0.409	0.012	0.434	0.013	0.443	0.013
Ti	0.006	0.005	0.003	0.001	0.004	0.001	0.003	0.001	0.003	0.001
Cr	0.001	0.001	0.001	0.001	0.001	0.001	0.001	0.001	0.000	0.001
Fe3+	0.019	0.022	0.056	0.020	0.042	0.023	0.057	0.015	0.051	0.027
Fe2+	0.144	0.022	0.098	0.019	0.091	0.023	0.069	0.018	0.084	0.025
Mn	0.002	0.002	0.001	0.001	0.001	0.001	0.001	0.001	0.001	0.001
Mg	0.492	0.013	0.400	0.009	0.471	0.014	0.456	0.014	0.445	0.010
Ca	0.583	0.009	0.473	0.012	0.556	0.009	0.496	0.012	0.482	0.010
Na	0.374	0.010	0.504	0.010	0.419	0.011	0.481	0.013	0.487	0.013
Jadeite	0.355	0.020	0.448	0.020	0.376	0.21	0.424	0.016	0.435	0.021
Aegirine	0.019	0.022	0.056	0.020	0.042	0.23	0.057	0.015	0.051	0.027
Augite	0.626	0.021	0.496	0.020	0.582	0.22	0.519	0.016	0.514	0.025
Estimated T	730–780°C		590–640°C		670–710°C		650–750°C		600–660°C	
Estimated P	>13 kbar		>12 kbar		>13 kbar		>13 kbar		>12 kbar	

σ: Standard deviations. Omphacites were analyzed by a Camebax SX-50 electron microprobe (accelerating voltage of 15 kV; beam current of 40 nA). Fe^{3+} was estimated considering a stoichiometry of 4 cations for 6 Oxygens. T and minimal P were estimated using the geothermometer of Ellis & Green (1979) and the Ab=Jd (in omph.) + Q equilibrium, with the solid solution model of Holland (1990).

tative of the various coaxial deformation types known to occur in eclogites. In the second part, we compare our results with those reported in the literature on both naturally and experimentally deformed cpx. The third part is devoted to the deformation mechanisms involved. Because omphacite rheology in eclogite is, to a first approximation, comparable to that of diopside in other cpx-bearing rocks, frequent references will be made to the latter in the course of discussion.

OMPHACITE MICROFABRICS

We have selected four eclogite samples representative of different coaxial strain types (from strongly-foliated to strongly-lineated, with varying intensity of strain). For each of these samples we have studied:

- the shape fabric;
- the crystallographic preferred orientation (CPO);
- the microstructures by light-optical and transmission electron microscopy techniques.

Description of the samples

The four studied eclogites are Seve78, Gal, G10 and C22.

Seve78 is an eclogite sample from Tjeliken mountain (Jämtland, Swedish Caledonides; location coordinates: 64°43'N, 14°44'E). For a geological description of the area, the reader is referred to Van Roermund & Bakker (1984) and Van Roermund (1985, 1989). Seve eclogites have a Finnmarkian age (505 Ma: Mørk *et al.*, 1988).

Gal is an eclogite sample from Cabo Ortegal (Galicia, Spain: 43°46'N, 7°53'W), and belongs to the Ibero-Armorican arc of the Hercynian belt. Eclogites from Cabo Ortegal have been described by Vogel (1967), Engels (1972), Kuijper *et al.* (1985) and Gil Ibarguchi *et al.* (1990). An age of 477 Ma has been obtained by Bernard-Griffiths *et al.* (1985).

G10 and *C22* are both from Les Essarts complex (Vendée, western France; grid reference Lambert II: G10: 306.10-2227.66; C22: 295.18-2234.12); they also belong to the Hercynian Ibero-Armorican arc. These eclogites and their geological setting have been described by Godard (1981, 1988). An age of 436 Ma has been obtained by Peucat *et al.* (1982).

These four eclogite samples contain the following primary high P mineral assemblage: omphacite, garnet, quartz and minor rutile. The omphacite composition ranges from Jd35 to Jd45 (Table 1) which is most common among omphacite compositions. These omphacites are unzoned and very homogeneous within one sample, as indicated by the low standard deviations (σ in Table 1). PT estimations give P>12 kbar and T=590 to 780 °C for eclogite formation (Table 1). Incipient retrogressive metamorphism is indicated by green amphiboles and oligoclase+diopside symplectites developed at the expense of omphacite.

Optical microstructures and shape fabrics

In the four eclogite samples, omphacite forms anhedral crystals with tabular shapes parallel to the lineation (L) and foliation (S) (Figs. 1 and 2). Results of omphacite shape fabric analyses are illustrated in a Flinn diagram (Fig. 5). The studied eclogites represent a range of omphacite shape fabrics that can be described as planar or strongly-foliated (S-type of Helmstaedt *et al.*, 1972) in Gal, linear or strongly-lineated (L-type of Helmstaedt *et al.*, 1972) in C22, and intermediate (SL- or LS-type) in Seve78 and G10.

Undulatory extinction, subgrain boundaries and infrequent ultra-thin deformation-twins are unevenly present in omphacite crystals. These microstructures are

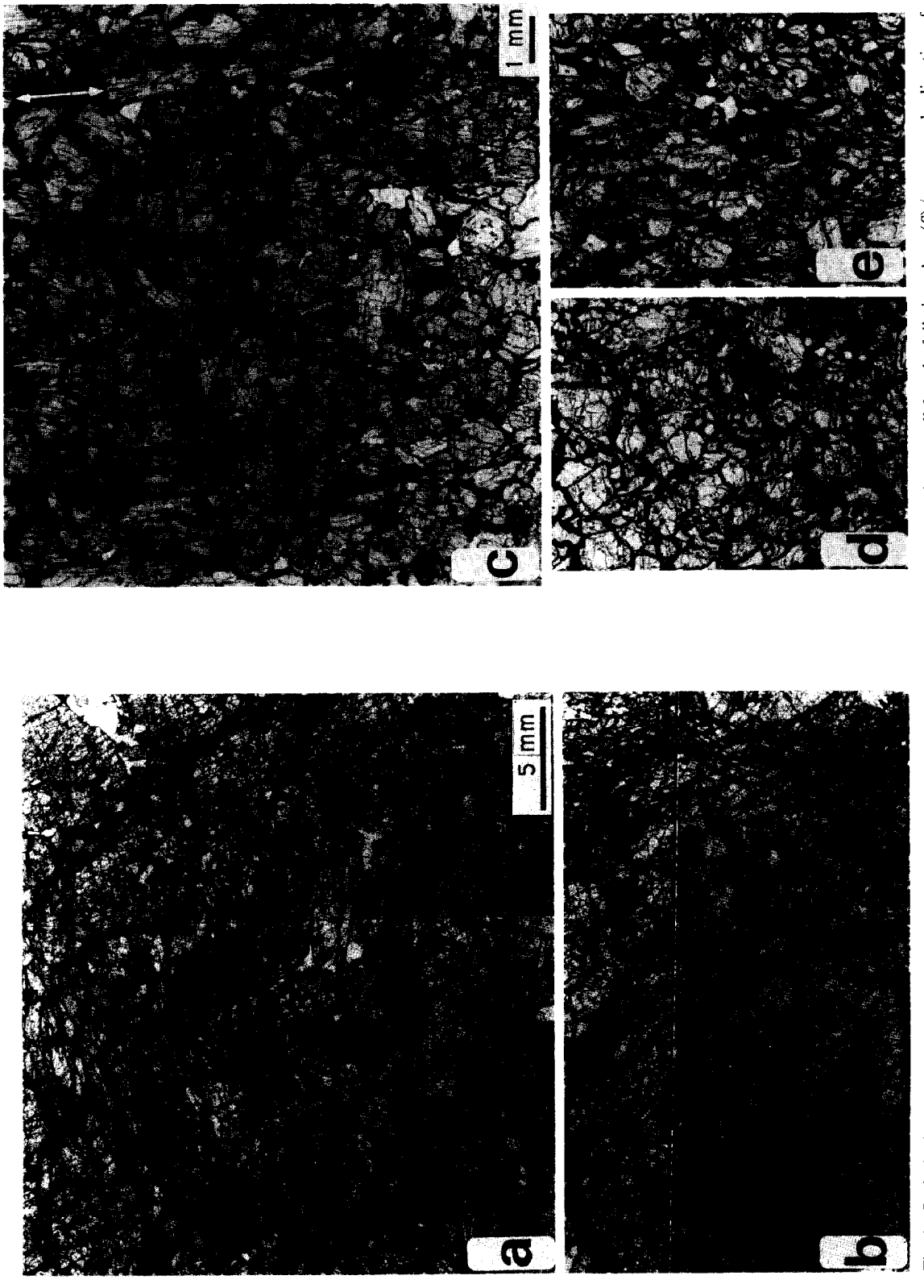

Fig. 1. Optical microstructures of eclogite samples C22 and Seve78. a, b: C22; c, d, e: Seve 78; a, c: sections parallel to the foliation plane (*S*) (arrow marks direction of lineation *L*); b, d: sections normal to the lineation (*L*); e: section perpendicular to *S* and parallel to *L*.

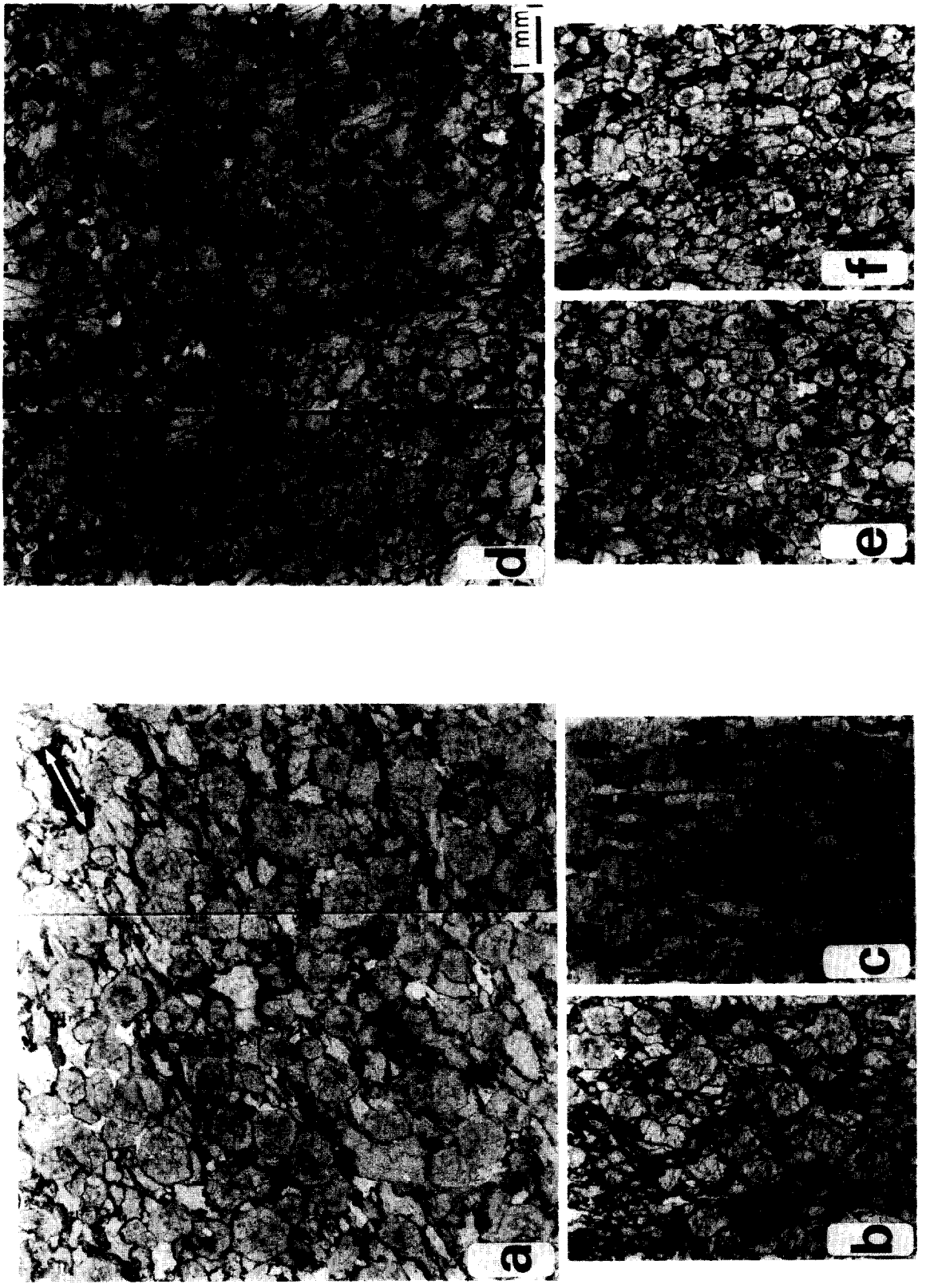

Fig. 2. Optical microstructures of eclogite samples G10 and Gal. a, b, c: G10; d, e, f: Gal; a, d: sections parallel to the foliation plane (S) (arrow marks direction of lineation L); b, e: sections normal to the lineation (L); c, f: sections perpendicular to S and parallel to L.

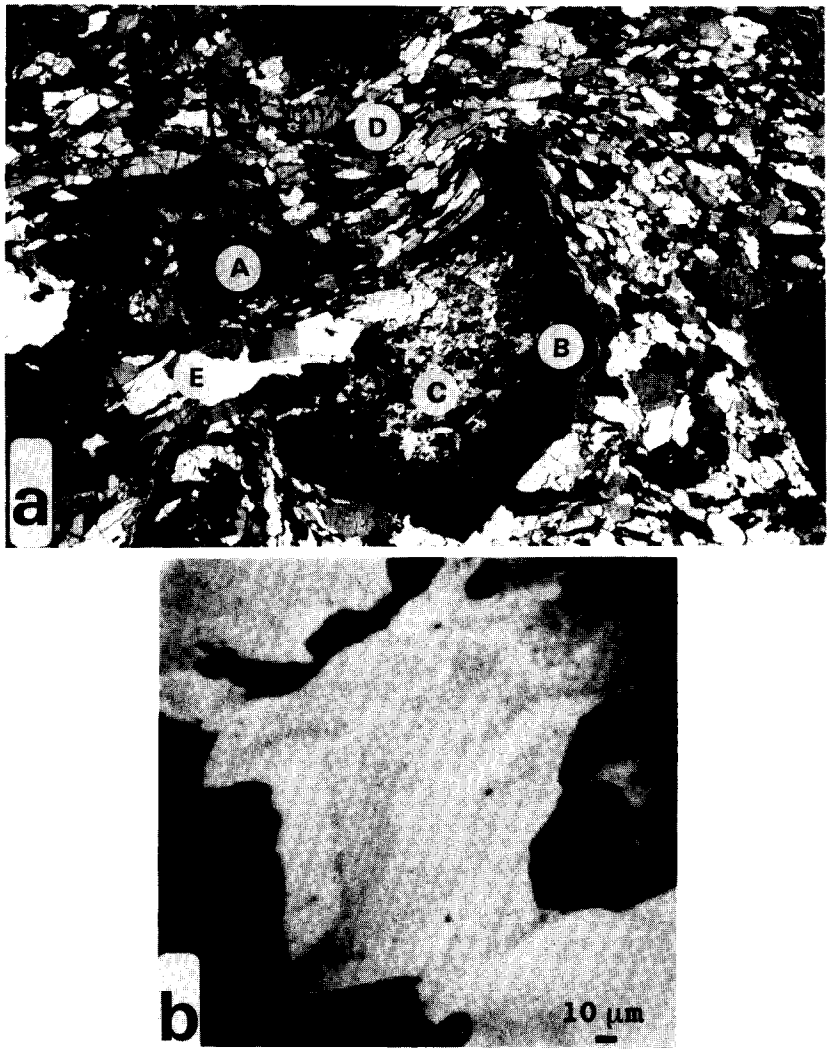

Fig. 3. (a) Omphacite and garnet microstructures (sample C22). (A) fragment of a garnet; (B) skeletal hollow garnet; (C) poorly-deformed micro-grained omphacite which has been sheltered from deformation by garnet (B); (D) strongly-deformed coarse-grained omphacite; (E) quartz. Note that a transition is visible between (C) and (D), and that the pyroxene-rich foliation in the (D) omphacite wraps round the (B) garnet.

(b) Syntectonic omphacite overgrowth. Ca X-ray map (256 grey levels). Sample described by Philippot & Van Roermund (1992). Dark grey: garnet; light grey: omphacite. Omphacite displays zones, the boundaries of which are parallel to the garnet boundaries, indicating omphacite overgrowth in response to grain boundary sliding effects.

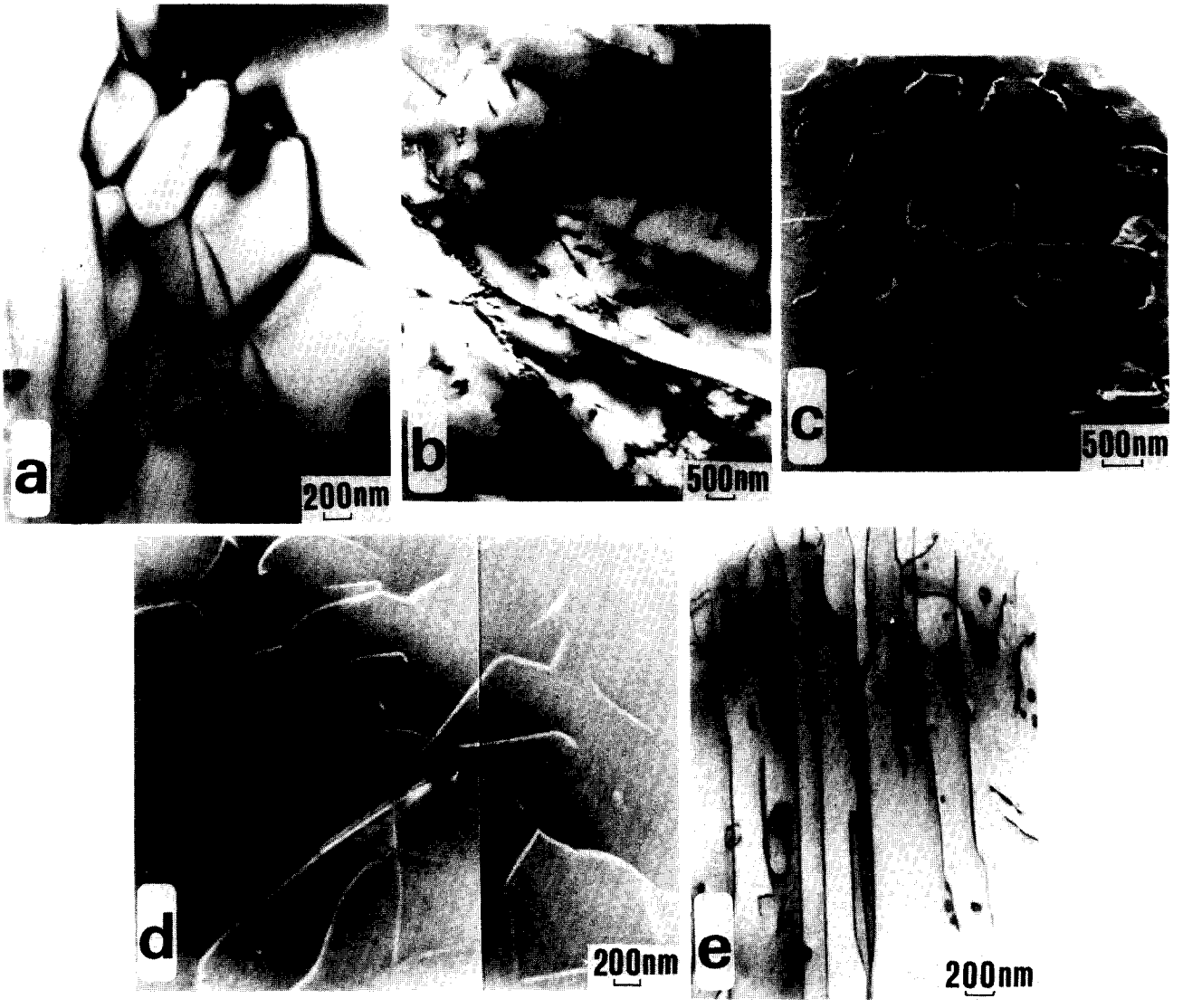

Fig. 4. Electron micrographs of dislocation substructures in omphacite. (a) Bright field (BF) electron micrograph showing a complex dislocation network in omphacite isolated in garnet (C22); (b) BF electron micrograph illustrating well-ordered dislocation subboundaries which delineate subgrains within a single larger omphacite grain (G10); (c) Dark field electron micrograph of isolated curved [001] dislocations, almost invisible ⟨110⟩ dislocations and local interactions between the two dislocation types (Ga1, g=(001)); (d) BF electron micrograph illustrating dislocation interaction patterns consisting of [001] and 1/2⟨110⟩ dislocations (G10); (e) Long straight [001] dislocations and isolated [001](100) loop (Ga1).

more abundant in Seve78 than in the other samples. In Seve78, the shape of the subgrains varies from equidimensional to elongated (size from 0.1 to 4 mm; aspect ratios 5:1). Subgrain boundaries, optically sharp and often curved, are generally sub-parallel to the crystal elongation. Most of the original omphacite grain boundaries are corroded by the late cpx+plagioclase symplectite and direct observation of their geometry is therefore not possible. However, indirect observations (Boland & Van Roermund 1983) indicate that in all cases omphacite grain boundaries were straight to slightly curved. Triple point junctions with interfacial angles of 120° are absent.

Subgrains and/or undulous extinction can be recognized locally also in some of the secondary amphiboles. Plagioclase of the late cpx+plagioclase symplectite after omphacite displays a few ultra-thin deformation-twins. Although both microstructures indicate a weak deformational overprint, these retrogressive minerals are clearly not elongated parallel to L and S and they do not display a fabric related to the main deformation event. The symplectite after omphacite, for example, is made of a fine intricate association of vermicules which are not expected to survive a strong deformation. Moreover, cpx+plagioclase symplectites sometimes nucleate along omphacite subgrain boundaries, indicating that omphacite deformation predated symplectite formation.

Commonly subhedral, the garnet crystals are not elongated and have the outlines of a rhombic dodecahedron. Their average size is about 2 mm, except for C22 in which they reach 1 cm (Figs. 1 and 2). Numerous observations indicate that garnets acted as rigid bodies, whereas omphacite deformed plastically. The pyroxene-rich foliation wraps around the garnet crystals which have preserved their subautomorphic shape. Unlike omphacite crystals, garnets display chemical zoning that would probably not have survived a diffusion-dependent plastic deformation. Moreover, in sample C22, some garnet crystals have been broken and became subsequently dispersed as isolated fragments within the omphacite matrix (Fig. 3a).

In sample C22, skeletal hollow garnet crystals have included, during eclogite formation, a part of the omphacite matrix (Godard 1988) (Fig. 3a). This polycrystalline omphacite isolated in a hollow garnet cavity does not have a strong fabric (Fig. 6: C22 inside Ga), unlike the omphacite present in the matrix of the same sample (Fig. 6: C22 matrix). It is fine-grained, very weakly oriented and full of minute inclusions of quartz and rutile, whereas the omphacite in the matrix is coarse-grained, strongly lineated and free of inclusions. This omphacite inside garnet is representative of an early stage in the eclogite evolution; it has escaped subsequent syn-eclogite-facies plastic deformation due to garnet's rigidity.

From the above observations, we can conclude that:

(a) the omphacite shape fabrics range from strongly-foliated S-types (Gal) to strongly-lineated L-types (C22), through intermediate SL (G10) and LS-types (Seve78);

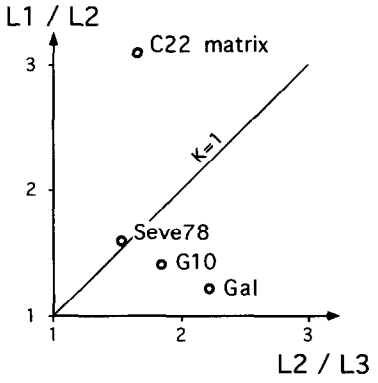

Fig. 5. Omphacite shape fabric analyses in a Flinn diagram. L1: mean crystal length in the direction parallel to L; L2: mean crystal length in the direction parallel to S and perpendicular to L; L3: mean crystal length in the direction normal to S.

(b) garnet behaved rigidly during plastic deformation;

(c) the main plastic deformation event took place before retrogression, i.e. in eclogite-facies conditions.

Crystallographic Preferred Orientation (CPO)

Omphacite crystallographic preferred orientations (CPOs) were measured on a 5-axes universal stage. To make cleavages more visible, uncovered thin sections were scratched with a needle before use.

The results (Fig. 6) reveal that [001] has a dominant orientation parallel to L while [010] has a dominant orientation normal to S. However, these general features undergo strong variations in relation to the shape fabric. Thus, in strongly-lineated samples (L-type: C22 matrix), [010] tends to be spread out in a great circle distribution normal to L, whereas [001] is dispersed in the S plane in the case of strongly-foliated samples (S-type: Gal). LS- and SL-types samples (G10 and Seve78) display intermediate features.

The polycrystalline omphacite included within a single hollow garnet crystal (C22 inside Ga in Fig. 6) clearly has a weaker CPO than the omphacite outside garnet (C22 matrix in Fig. 6). This confirms that the isolated omphacite has been sheltered from plastic deformation. Moreover, the omphacite CPO inside garnet has no relationship with the external S and L. This illustrates that this garnet has been rotated relative to the matrix and behaved as a rigid body during deformation.

Figure 6 also illustrates that [001] and [010] are roughly symmetrically arranged with respect to L and S. A small asymmetry occurs in the case of sample C22 due to the following artefact: the large garnets in this sample (up to 1 cm: Fig. 2) cause local changes in the L and S orientations as these wrap around the garnet. Such minor deviations have not been taken into account.

So far, cpx CPOs have been illustrated using traditional [100], [010] and [001] pole figures (Fig. 6). Each pole figure represents only one particular axis and, in this way, part of the information is lost since correlation between axes of a particular crystal is impossible. In

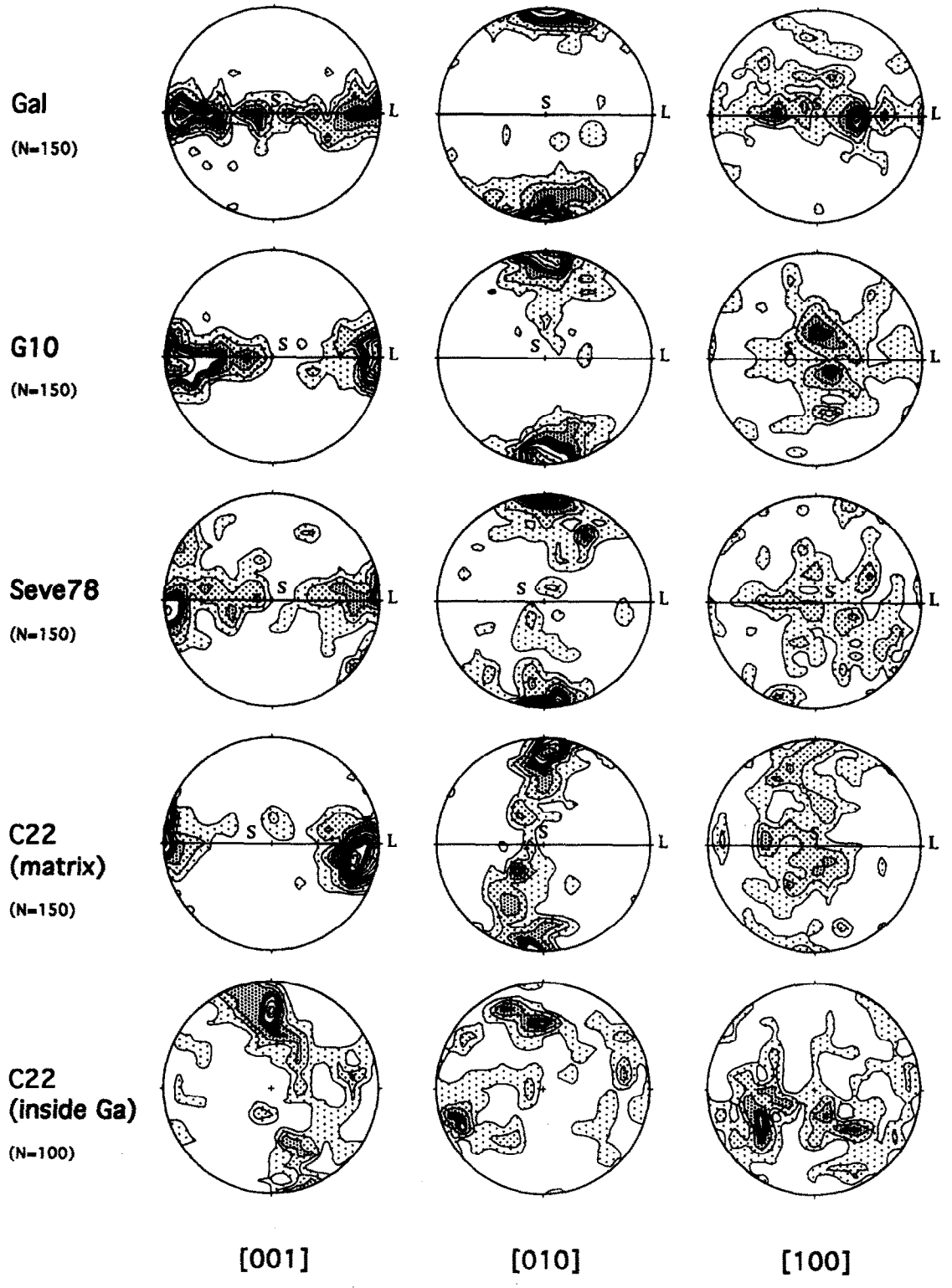

Fig. 6. Omphacite Crystallographic Preferred Orientations (CPOs). Equal area projection in the lower hemisphere. Contours are 1, 2, 3, 4, 5, 6, 7, 8, 9, 10, 15% per 1% area. Foliation plane (S) is vertical EW. Lineation direction (L) is horizontal EW. N: number of measurements.

addition, no information is presented about the CPOs of other axes which might nevertheless define stronger maxima. To avoid these problems, we have used two different methods, the results of which are presented in Figs. 7 and 8.

The first method uses Bingham statistics (e.g. Mardia 1972, Bingham 1974, Allmendinger 1988): one direction in the three-dimensional space is a vector that can be represented by its three direction cosines, taken as coordinates. For one particular axis distribution, we can calculate the 3×3 covariance matrix of the direction cosines. This matrix can be diagonalized and thus gives three eigenvalues and three corresponding eigenvectors. The three eigenvectors obtained represent the

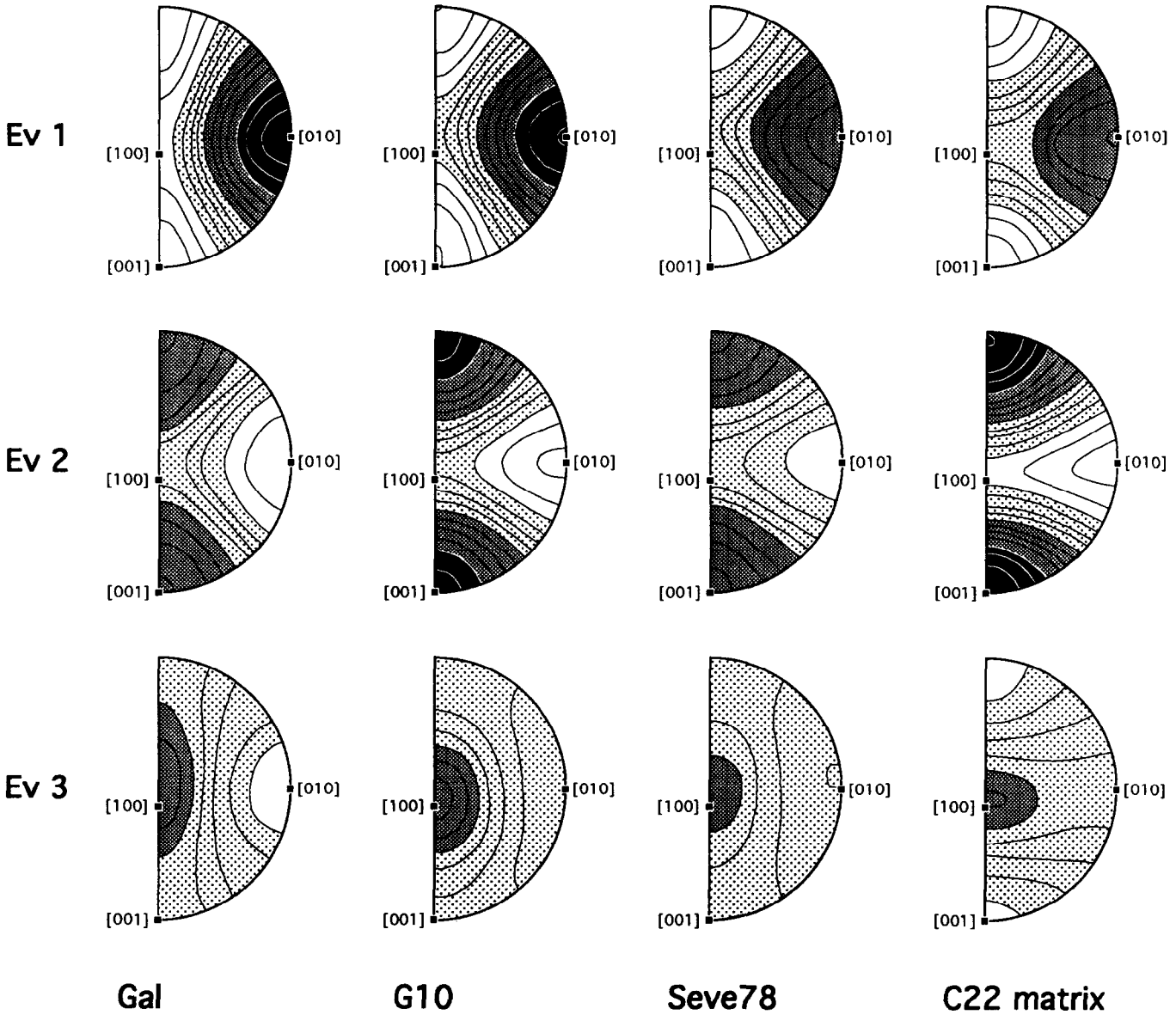

Fig. 7. Eigenvalues of the Bingham statistics contoured in the crystallographic reference frame. Eigenvalues are normalized to 1 (see text). Equal angle projection in the lower hemisphere. Contour interval is 0.05. White: 0–0.2; light grey: 0.2–0.4; dark grey: 0.4–0.6; black: 0.6–0.8.

three canonic axes of the distribution: the best fit axis, the perpendicular to the best fit axis in the best fit great circle, and the pole to the best fit great circle. The three eigenvalues, normalized to 1, give a measure of the importance of the corresponding eigenvectors and thus characterize the distribution type. For example, a point concentration will have one large eigenvalue and two much smaller ones. A girdle concentration will have two equal eigenvalues; the third will be almost null. Finally, a uniform distribution will have three approximately equal eigenvalues. We have computed these eigenvalues from the distribution of 450 different crystallographic axes in omphacite and the results, plotted and contoured in the crystallographic reference frame, are presented in Fig. 7. Because of the omphacite monoclinic symmetry, distinction between axes [hkl] and [h$\bar{k}$l] is impossible, and the figures are symmetric relative to the (010) plane. The results show that, in all cases, the crystallographic axes with the strongest preferred orientations are [001], [010] and a^* (directional normal to (100)). Moreover, it again demonstrates that the [001] CPO forms the strongest maximum in the L-type sample (C22 matrix), while [010] CPO forms the strongest maximum in the S-type eclogite (Gal).

The second method consists of representing the orientation distribution (OD) in the three-dimensional Euler space (Wenk & Wilde 1972, Bunge 1981, 1985). The three coordinates of one point of the Euler space represent the three Euler angles that completely characterize one rotation in the real space. Since one particular crystal orientation can be expressed as a rotation from a reference orientation to the actual orientation, it can be represented by one point in the Euler space. During OD calculations, we used Bunge's definition of Euler angles ($\psi 1$, ϕ, $\psi 2$) and we chose, as the origin in the Euler space, the null rotation for which the actual orientation

coincides with the reference orientation defined by the following Ka and Kb:

(a) Ka (the sample coordinate system): mean [001] as x; mean [010] as y; mean a^* as z (we chose mean crystallographic directions rather than S and L directions, in order to avoid the artefact due to the garnet size: see above).

(b) Kb (the crystal coordinate system): [001] as $-x$; [010] as y; a^* as $-z$.

Because of the monoclinic symmetry, one single orientation can be expressed as two different rotations and is thus represented by two symmetric points in the Euler space. For the sake of convenience, points of the $\psi1$–ϕ–$\psi2$ Euler space have been projected onto the $\psi1$–$\psi2$, $\psi1$–ϕ and $\psi2$–ϕ planes (Fig. 8). To facilitate the interpretation of the OD patterns, we plotted the effect of consecutive rotations of 10° about [001] or [010] axes (model in Fig. 8). By comparing the model and the patterns, it can be seen that the OD of the strongly-foliated sample (Gal) is characterized by a dominant rotation about [010], while a dominant rotation about [001] characterizes the OD of the strongly-lineated sample (C22). The ODs of Seve78 and G10 display intermediate features revealing the effects of both rotation axes. The increase in the CPO intensities, from C22 (inside garnet), Seve78, G10, up to Gal and C22 (matrix), is also revealed by OD patterns.

From the omphacite CPO studies, we can conclude that:

(a) [001] tends to be parallel to L while [010] tends to be normal to S;

(b) CPO patterns range between two extreme types which can be described in terms of rotation about [001] and [010], these axes having the strongest preferred orientations. The CPO type (centered on [001] or [010]) is correlated with the shape fabric type (from L-type to S-type, respectively) and is indicative for the type of strain (from pure constriction to pure flattening, respectively);

(c) there is also a correlation between the intensity of the shape fabrics and that of the CPOs.

TEM microstructures

In all cases, the microstructure observed by transmission electron microscopy (TEM) consists of a range of planar defects and a variety of dislocation substructures: isolated curved free dislocations; isolated long-straight dislocations; isolated loops; isolated nodal points; tiltwalls; complex dislocation networks; (100) microtwins; (010) planar faults and antiphase domains (Fig. 4).

The basic dislocation substructure, in all samples except Gal, consists of various types of dislocation walls which delineate subgrains within larger grains (Figs. 4a & b). Subgrain domains contain a low density of free dislocations; some in fact have none. Free dislocations may have interacted to form nodal points or junctions; others are curved or form loops. Subgrain sizes appear to be irregular. The geometry of the subgrain boundaries varies from simple tiltwall configurations to more complicated dislocation networks involving dislocations with three different Burgers vectors. This TEM microstructure is indicative of dislocation creep processes, i.e. dislocation glide and climb processes are concomittant with subgrain boundary migration. In the Gal sample, well-defined subgrain boundaries have not been observed (Fig. 4c). Here, the dislocation substructure consists of fairly homogeneously distributed isolated and curved free dislocations (Burgers vector=1/2⟨110⟩ and [001]) that have frequently interacted to form isolated nodal points or some extended version of this (Fig. 4c). Detailed analyses of some isolated nodal points and loops indicate however that the dislocation systems are similar to those in the other samples.

In contrast with omphacite, well ordered dislocation networks are absent in the late symplectitic cpx after omphacite. This confirms that symplectite formation during retrogression postdates the dislocation creep process. Some symplectitic cpx however contain unidentified scarce isolated dislocations.

Contrast analyses indicate that dislocations in omphacite have Burgers vectors 1/2⟨110⟩, [001] and 1/2⟨112⟩. Dislocations with Burgers vector 1/2⟨112⟩ are only present in networks and are attributed to the dislocation reaction 1/2⟨110⟩ + [001] → 1/2⟨112⟩ (Van Roermund & Boland 1981). The variable dislocation line directions of isolated curved dislocations do not specify particular crystallographic planes. In contrast, dislocation loops are present in (100) and {110} planes. Dislocation loops in (100) have Burgers vector [001] and define the slip system [001](100) (Fig. 4e). However, these [001] loops are always associated with isolated long-straight [001]-dislocations (dominantly [001]-screws) that occur in particular zones, often parallel to (100). These zones have tentatively been interpreted as being the result of some late, but minor, deformation effect. Loops in {110} have Burgers vector 1/2⟨110⟩ and [001]; consequently, these loops define the slip systems 1/2⟨110⟩{$\bar{1}$10} and [001]{110}. Finally, in samples G10 and C22 (matrix), omphacite grains having high dislocation densities are adjacent to omphacite grains in which dislocation densities are low.

The following planar defects have been identified: (100) deformation twins, (010) planar defects (Fig. 4c) and antiphase domain (APD) boundaries. APDs formed when omphacite evolved from a disordered C2/c to an ordered P2/n state, probably during retrogressive metamorphism (Carpenter 1979, Rossi 1988). Their formation postdates the dislocation creep process as dissociated 1/2⟨110⟩ dislocations (Van Roermund & Lardeaux 1991) are absent. APD sizes are widely variable and range from 300 Å in sample Gal to 3500 Å in sample C22 (Van Roermund, 1992). Due to their infrequent occurrence, (100) deformation twins and (010) planar defects have not been analysed any further.

From the TEM microstructural studies, we can conclude that:

(a) dislocation creep occurred during plastic deformation, before retrogressive metamorphism;

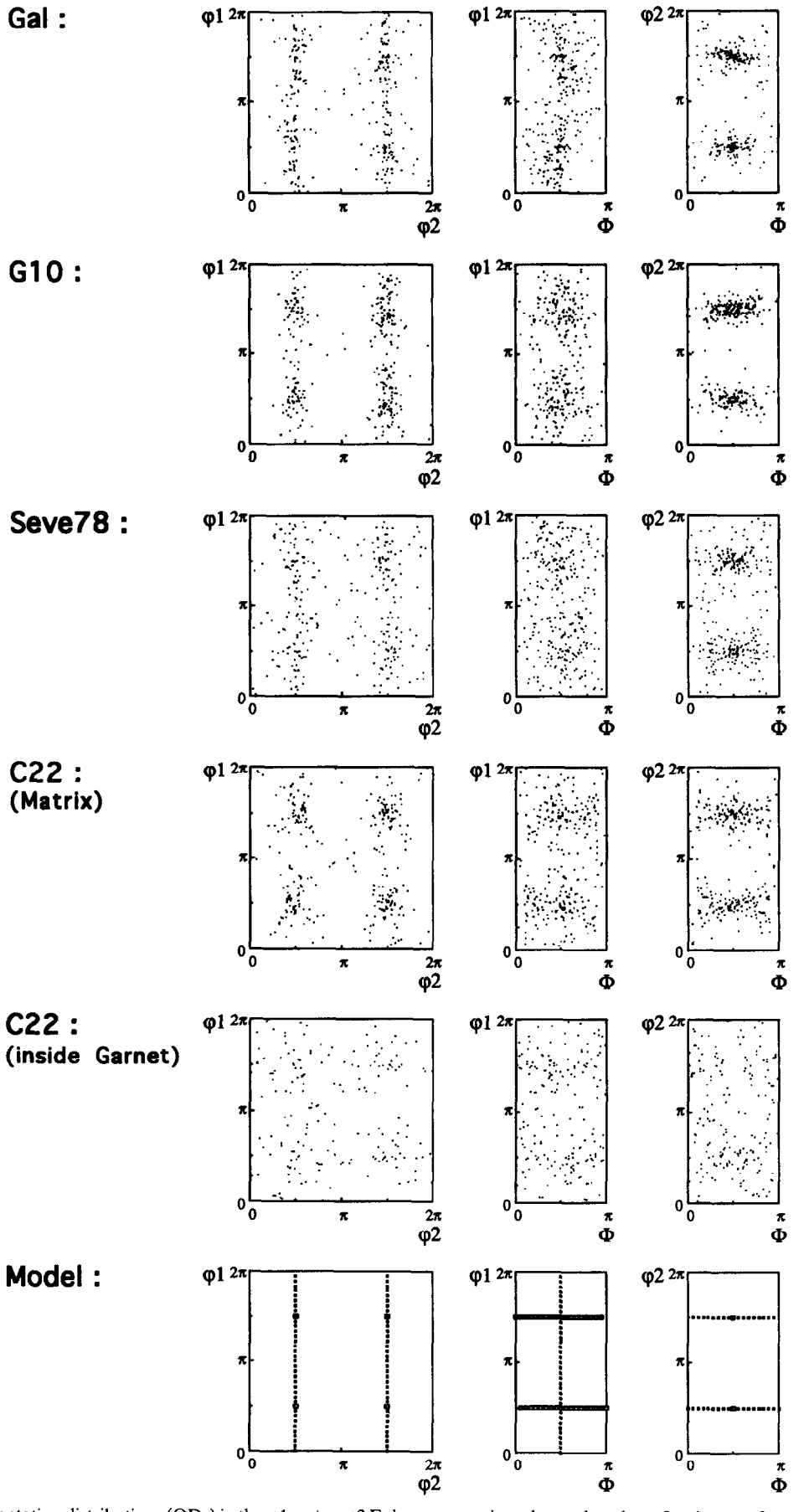

Fig. 8. Orientation distributions (ODs) in the $\psi 1 - \phi - \psi 2$ Euler space projected onto the $\psi 1 - \psi 2$, $\psi 1 - \phi$, $\psi 2 - \phi$ Euler planes. Same data as in Fig. 6. Model: Open squares represent 10° rotations about [010]; full squares represent 10° rotations about [001] (see text).

Table 2. Type of defects in cpx reported in the literature

Sources	Material	Conditions		Slip systems			Twin systems	
Griggs *et al.* (1960)	diopside clinoenstatite	exp.	OM	**(100)[001]**			(100)[001]	(001)[100]
Raleigh & Talbot (1967)	diopside	exp.	OM	**(100)[001]**			(100)[001]	(001)[100]
Kirby & Christie (1967)	diopside	exp.	TEM				(100)1/2[001]	(001)[100]
Avé Lallement (1978)	diopside	exp.	OM	(100)[001] (100)[00$\bar{1}$]	{1$\bar{1}$0}⟨110⟩ {$\bar{1}$11}⟨110⟩ (001)⟨110⟩	(102)[201]	(100)[001]	rare (001]
Van Roermund & Boland (1981)	omphacite	nat.	TEM	(100)[001] {110}[001]	{$\bar{1}$10}1/2⟨110⟩	1/2⟨112⟩	(100)	
Kollé & Blacic (1982)	diopside hedenbergite	exp.	TEM	(100)[001]			(100)[001]	(001)[100]
Van Roermund (1983, 1984)	omphacite	nat.	TEM	(100)[001] {110}[001]	{$\bar{1}$10}1/2⟨110⟩	1/2⟨112⟩	(100)	(001)
Kirby & Kronenberg (1984)	diopside hedenbergite	exp.	TEM	**(100)[001]**			(100)	(001)
Van Duysen & Doukhan (1984)	spodumene	exp. (<400°C)	TEM			(100)[010]	(100)	(001)
Van Duysen & Doukhan (1984)	spodumene	nat.	TEM	{110}[001]	{1$\bar{1}$0}1/2⟨110⟩			
Boland & Tullis (1986)	diopside	exp.	TEM	[001]	1/2⟨110⟩	1/2⟨112⟩		
Buatier *et al.* (1991)	omphacite	nat.	TEM	(100)[001] {110}[001]	{$\bar{1}$10}1/2⟨110⟩		(100)	
Raterron & Jaoul (1991)	diopside	exp.(>1000°C)	TEM		**{$\bar{1}$10}1/2⟨110⟩**			
Philippot & Van Roermund (1992)	omphacite	nat.	TEM	(100)[001] {110}[001]	{$\bar{1}$10}1/2⟨110⟩	(010)[100]	(100)	(001)
Ingrin *et al.* (1992)	diopside	exp.	TEM	(100)[001] (010)[001]	**{$\bar{1}$10}1/2⟨110⟩**			
Raterron *et al.* (1994)	diopside	exp.(>1000°C)	TEM	{110}[001]	**{110}1/2⟨110⟩**	(100)[010]		
Skrotzki (1994)	augite	nat.	TEM	**(100)[001]**	**{110}1/2⟨110⟩**	(100)[010] {110}1/2⟨112⟩ (010)[100] (010)⟨101⟩ {110}⟨111⟩		
This study	omphacite	nat.	TEM	(100)[001] {110}[001]	{$\bar{1}$10}1/2⟨110⟩	1/2⟨112⟩	(100)	

exp.: Experimentally strained cpx; nat.: naturally strained cpx; OM: observation by optical microscopy; TEM: observation by transmission electron microscopy. Dominant slip systems are shown by bold type.

(b) the operative slip systems were: [001](100); 1/2⟨110⟩{$\bar{1}$10} and [001]{110}.

OTHER STUDIES ON CLINOPYROXENE DEFORMATION

Naturally deformed cpx

A large number of naturally deformed cpx fabrics have been reported. They can conveniently be classified by the dominant crystallographic plane parallel to S:

(a) (010) fabrics: These are the commonest cpx fabrics and they are similar to those described in the present study: [001] is close to L and [010] is more or less normal to S, but strong variations are seen in relation to the strain type (from L- to S-type: see above). Such CPOs seem to be frequent in rocks of deep origin. They have been reported from numerous eclogites (Kozlowski 1965, Binns 1967, Kumazawa *et al.*, 1971, Baker & Carter 1972, Carter *et al.*, 1972, Engels 1972, Helmstaedt *et al.*, 1972, Von Herrmann *et al.*, 1979, Godard 1981, Van Roermund 1983, Godard 1988, Van Roermund 1992, Boundy *et al.*, 1992). Similar CPOs have also been described for pyroxenic layers within peridotite (Yoshino 1961, 1964, Carter *et al.*, 1972, Boudier 1978, Barruol & Mainprice 1993), for cpx-bearing peridotites (Avé Lallement 1967, Möckel 1969), cpx-bearing granulites (Kozlowsky 1965, Engels 1972, Van Zuuren 1969) and a sheared gabbro (Barruol & Mainprice 1993).

(b) (100) fabrics: in this type, [001] is close to L and a^* is perpendicular to S. [010] is thus perpendicular to L but lies in the S plane instead of being normal to S. This infrequent cpx CPO seems to occur in low-T mylonitic rocks: annealed mylonitic low-T eclogite of Philippot & Van Roermund (1992); 'mylonitic pyroxenite' and 'cpx-gt mylonitic amphibolite' of Ji *et al.* (1993). This fabric type is otherwise rare in cpx but is common for orthopyroxenes (Mercier 1985, Mainprice & Nicolas 1989).

(c) (010)+(100) fabrics: some rocks display two [010] maxima, one in the S plane perpendicular to L and the other normal to S, while [001] is parallel to L: aegirine augite-bearing schists of Kojima & Hide (1957); cpx-bearing amphibolite of Inoue (1961); Jd10 'eclogite' of Kappel (1967). They can be described as having intermediate CPOs between the two previous types.

(d) Finally, some rare rocks with minor cpx display a [001] concentration perpendicular to L and parallel to S: cpx-bearing amphibolite of Siegesmund *et al.* (1989); 'mafic ultramylonite' of Ji *et al.* (1993).

TEM studies on naturally deformed omphacite from eclogite have been conducted by Lorimer *et al.* (1972), Champness *et al.* (1974), Van Roermund & Boland (1981), Van Roermund (1983, 1984), Buatier *et al.* (1991), Van Roermund & Lardeaux (1991), and Philippot & Van Roermund (1992). Their results on operative slip system analyses have been listed in Table 2. The most common slip systems are 1/2⟨110⟩{$\bar{1}$10}, [001]{110} and [001](100), while [100](010) has only been identified in eclogites deformed at low T (Philippot & Van Roermund 1992).

Table 3. Experimentally determined constants for power law flow in cpx and clinopyroxenites

Sources	Material	Conditions	Parameters A (kJ/mol)	n	Q	Time (Ma) to get 50% strain T = 600°C σ = 100 MPa	600°C 500 MPa	900°C 100 MPa	900°C 500 MPa
Monocrystals									
Avé Lallement (1978)	Diopside		7.94 e−5	4.3	284	*4.8 e+4*	*47*	**2.2**	**2.2 e−3**
Kollé & Blacic (1983)	Hedenbergite		2.00 e+8	3.6	526	*1.4 e+8*	*4.3 e+5*	**1.3**	**3.8 e−3**
Raterron & Jaoul (1991)	Diopside	Orientation 1	1.58 e−8	6.5	442	*3.2 e+13*	*9.9 e+8*	*5.6 e+6*	*1.7 e+2*
Raterron & Jaoul (1991)	Diopside	Orientation 2	3.16 e+8	8.1	742	*8.4 e+11*	*1.9 e+6*	**3.8**	**8.7 e−6**
Polycrystals									
Avé Lallement (1978)	Websterite	Dry	3.98 e−7	4.3	327	*3.6 e+9*	*3.5 e+6*	*3.6 e+4*	**35**
Avé Lallement (1978)	Websterite	'Wet', high strain	1.99 e−5	5.3	382	*1.4 e+9*	*2.7 e+5*	*2.0 e+3*	**0.39**
Avé Lallement (1978)	Websterite	'Wet', low strain	3.16 e+3	3.3	463	*6.1 e+9*	*3.0 e+7*	*5.1 e+2*	**2.5**
Kirby & Kronenberg (1984)	Clinopyroxenite	Dry, high T	1.00 e−4	5.3	380	*2.1 e+8*	*4.1 e+4*	*3.2 e+2*	**6.4 e−2**
Boland & Tullis (1986)	Clinopyroxenite	'Wet'	1.48 e+5	3.3	490	*5.3 e+9*	*2.6 e+7*	*1.7 e+2*	**0.85**

A, n, Q: constants of the power law (equation 1). Time (Ma) involved to produce 50% strain for given temperatures and stress magnitudes (in italics: unrealistic values).

Experimentally deformed cpx

Experimental cpx deformation studies have been performed by a number of researchers using various experimental deformation techniques (under confining pressure, Griggs, gas or dead load apparatus). These experiments were performed either on single crystals (diopside, hedenbergite: Hornemann & Mueller 1971, Avé Lallement 1978, Kollé & Blacic 1982, 1983, Doukhan *et al.*, 1985, Raterron & Jaoul 1991, Ingrin *et al.*, 1991, 1992, Raterron *et al.*, 1994; spodumene: Van Duysen & Doukhan 1984), or on polycrystalline aggregates (eclogites: Rummel 1969, Ryabinin *et al.*, 1973, Jakubith & Seidel 1982; clinopyroxenites, websterites: Raleigh & Talbot 1967, Carter *et al.*, 1972, Kirby & Christie 1977, Avé Lallement 1978, Kirby & Kronenberg 1984, Boland & Tullis 1986).

Results indicate that, under sufficient confining pressure to avoid brittle deformation, two strain regimes can be identified in the case of diopside:

(a) A low T/high strain rate regime in which plastic strain is accommodated by mechanical twinning on (001) and (100), accompanied by [001](100) slip (Avé Lallement 1978, Ashworth 1980). The critical resolved shear stress for twinning is almost insensitive to T and strain rate variations (Kollé & Blacic 1982, 1983).

(b) A high T/low strain rate regime in which the strength drops rapidly with increasing T/decreasing strain rate. Plastic strain is accommodated by multiple slip involving 1/2⟨110⟩{$\bar{1}$10}, [001](100), [001]{110} and/or [100](010) (Table 2). According to Raterron & Jaoul (1991) and Raterron *et al.* (1994), 1/2⟨110⟩{110} is dominant at high T, while [001](100) is the easiest system at intermediate T. Polygonisation and recrystallisation are obvious. Deformation and recrystallisation in aggregates are both promoted by addition of water (Boland & Tullis, 1986).

Within the high T/low strain rate regime, the experimentally derived flow data have been satisfactorily fitted using an Arrhenius law:

$$\dot{\varepsilon} = A\,\sigma^n \exp(-Q/RT) \qquad (1)$$

where $\dot{\varepsilon}$ is the strain rate, σ is the axial compressive stress and Q is the activation energy. The experimentally derived values for parameters A, n, and Q, obtained by various authors, are listed in Table 3.

An experimentally produced cpx CPO has been reported by Carter *et al.* (1972). This CPO is a (010) *S*-type fabric, [010] being concentrated parallel to the uniaxial compression direction.

OMPHACITE DEFORMATION MECHANISMS

Plastic deformation and crystallographic mineral fabrics can be produced by several different processes: twinning; dislocation creep; recrystallization and grain boundary mobility.

Twinning

Experiments on cpx have demonstrated that twinning is only a major deformation process at low T and/or very high strain rates. Twins are thus very abundant in shocked cpx from meteorites (Ashworth 1980, 1985) but in eclogites, on the other hand, the twin density is always low and the finite strain due to twinning can be neglected. Some (100) microtwins were observed in the present study and twins visible by the optical microscope very seldom occur in some large centimetric omphacites (Godard 1988).

Dislocation creep

The observed isolated dislocations and well-ordered dislocation walls in omphacite demonstrate that dislocation glide and climb (creep) have been operative in the studied samples.

Models concerned with the formation of crystallographic mineral fabrics by dislocation glide and/or creep processes have been conveniently classified into the two following end-members (Wenk & Christie 1991 and refs therein):

(a) The first end-member is based on the *stress equilibrium* condition. Only the easiest activated slip system is operative. This end-member is therefore called single

slip model, or 'lower bound' critical resolved shear stress (CRSS) model. It has been successfully applied to the interpretation of mineral CPOs formed in polycrystalline aggregates where low-symmetry minerals deform dominantly by dislocation glide on a single slip system, e.g. phyllosilicates, olivine and ice (Bouchez 1977, Etchecopar 1977, Wilson 1986, Etchecopar & Vasseur 1987). This model implies the creation of an heterogeneous stress distribution around or within the individual grains because homogeneous strain in a polycrystalline aggregate can only be produced when five independent slip systems are activated (Von Mises (1928) criterion). To keep material coherency during deformation, the model has to put limits on the differential stress levels that can be produced within the deforming material. The boundary conditions are therefore 'stress equilibrium'. CPOs are generated by lattice rotations due to slip along the single glide plane and by mechanical grain rotation, imposed on the grain by its neighbours in order to maintain the stress equilibrium condition. Numerous studies have demonstrated that large strains produce a rotation of the slip plane into parallelism with S, while the slip direction rotates towards L.

(b) The second end-member model assumes *strain compatibility* obtained by the operation of five independent slip systems. As five slip systems have to be activated simultaneously, this model refers to an 'upper bound' CRSS situation and is called multiple slip model. Phases with high symmetry (metals, calcite) deform in this way. The model involves homogeneous deformation at all scales. In order for the mineral aggregate to deform homogeneously, each individual crystal ought to be able to fully accommodate the imposed strain. This happens because five independent slip systems are operative (Von Mises (1928) criterion). In contrast to the single slip model, the boundary conditions set by the strain-compatibility criterion implies that mechanical rotation of grains is absent, i.e. crystal lattice rotations are entirely due to the dislocation glide process.

Depending on the number of operative independent slip systems, intermediates between these two models occur. New model approaches, like the viscoplastic self-consistent theory of Molinari *et al.* (1987) can be regarded as a kind of combination of these two end-member models.

The low symmetry argument has been used to apply the single slip model to cpx-bearing rocks (Nicolas & Poirier 1976, Mercier 1985, Mainprice & Nicolas 1989). According to these authors, (100) and (010) cpx fabrics were formed by dominant [001](100) and [001](010) slip respectively. However, [001](010) has never been identified as a dominant slip system in naturally or experimentally deformed cpx (Table 2). Thus, multiple slip, involving $1/2\langle 110\rangle\{\bar{1}10\}$, $[001]\{110\}$ and $[001](100)$, is a more likely candidate to explain the common (010) fabrics (Van Roermund 1984, Buatier *et al.*, 1991, Van Roermund 1992). However, several questions arise in considering this hypothesis:

(a) Von Mises criterion is not completely fulfilled as only three independent slip systems operate. This is intuitively related to the fact that none of the slip systems intersect the tetrahedron chains. Thus, for some particular crystallographic orientations, strain cannot be accommodated by slip and another process must also be involved. In addition, the multiple slip model assumes homogeneous deformation, and the rigidity of the garnet crystals introduces an inhomogeneous deformation component.

(b) In the case of single slip, the slip direction and plane rotate towards L and S, respectively. The effect of multiple slip on cpx CPO is more difficult to model. [001] axis parallel to L can be explained if slip systems whose Burgers vector is [001] are dominant. On the other hand, when two equivalent slip planes are operating, the crystal rotates and reaches a position of equilibrium where the resolved shear stresses on both planes are equal. In the case of cpx, both [010] and a^* should define maxima normal to S, as these two axes are almost equivalent bisectors relative to the two $\{110\}$ slip planes (cleavages) which are almost orthogonal (93°) and have the same critical resolved shear stress. Thus, one should expect two maxima of the [010] axis, one normal to S and the other perpendicular to L in the S plane. This occurs in very few rocks ((010)+(100) fabric, see above) but, in most of the cases, only the first of these expected maxima exists ((010) fabric). Moreover, the operation of the third common [001] (100) slip system would favour the missing maximum. Therefore, the multiple slip hypothesis cannot explain all aspects of the cpx CPOs. It would imply the intervention of another mechanism which selectively eliminates one of the expected [010] maxima.

(c) Eclogite-facies temperatures usually range from 500 to 800 °C, and the extrapolated creep laws for diopside clearly indicate that at T below 700 °C it becomes impossible to accommodate strain by dislocation creep since unreasonable high stresses or slow strain rates have to be proposed (Table 3). However, diopside may not be a good rheological analogue for omphacite. Differences in chemistry may result in changes in defect behaviour and hence in rheological laws. Moreover, creep laws are sensitive to T_{melt}. Data on melt along the diopside-jadeite join (Yoder 1952, Bell & Davis 1969, Williams & Kennedy 1970, Biggar 1972, Litvin & Gasparik 1993) indicate that Jd40-Di60 omphacite melts at about 200 °C below pure diopside and the true creep law for this composition must be shifted to lower T compared to that for diopside. High pressure, on the other hand, has the opposite effect on T_{melt} ($\Delta T \approx +100$ °C for $\Delta P = +10$ kbar) and hence on the creep law. In spite of these uncertainties, it seems that dislocation creep becomes poorly efficient at some low-T eclogite-facies conditions ($T < 500$ °C) and other deformation mechanisms may compete with it.

In addition, relics of coesite included in omphacite (e.g. Smith 1984) indicate that the increase in volume due to the coesite-quartz transition ($\Delta V/V \approx +0.08$) is not completely accommodated by plastic deformation of omphacite. The inclusions induced a local elastic over-

pressure (Gillet *et al.*, 1984, Van Der Molen & Van Roermund 1986) and produced some brittle deformation (radial cracks) in the host omphacite. Since intracrystalline diffusion in omphacite is needed for increasing the volume of isolated inclusions, this indicates that mechanisms such as creep or mass transfer by *intra*-crystalline diffusion have a limited efficiency. They are however more efficient in omphacite than in garnet where relics of coesite are more frequent.

Dynamic recovery and rotation recrystallization

Dislocation creep and polygonization can generate a well-defined subgrain structure within omphacite grains. Subboundaries, subparallel to the (010), (100) or {110} planes, consist of complex dislocation networks (Van Roermund & Boland 1981, Van Roermund 1984, Buatier *et al.*, 1991, this study). Through progressive misorientation, subgrains evolve to independent grains, i.e. old omphacite porphyroclasts generate neoblasts of a much smaller size. Some low-T eclogites (Kappel 1967, Van Roermund 1984, Péquignot *et al.*, 1984, Bouchardon 1989, Buatier *et al.*, 1991, Philippot & Van Roermund 1992) display microstructures characteristic of this phenomenon which has been studied in detail by Buatier *et al.* (1991). This omphacite microstructure seems to be restricted to eclogites deformed at $T \leq 600$ °C. Kappel (1967), Buatier *et al.* (1991) and Philippot & Van Roermund (1992) showed that the neoblast CPO is weaker but similar to that of the porphyroclasts, i.e. new strong CPOs do not develop by this mechanism.

Dynamic grain boundary mobility and crystal growth

Deformation-induced grain boundary mobility seems to play an important role in cpx. In sample C22, for example, crystal growth obviously occurred during deformation. The deformed matrix omphacite crystals are considerably larger than the poorly deformed ones isolated in a hollow garnet. The latter are approximately 13 times more numerous per unit volume than the former (Godard 1988). A transition in size and shape between the two omphacite populations can be observed (Fig. 3a). Growth of omphacite neoblasts during dynamic recrystallization has also been suggested by Champness *et al.* (1974), Buatier *et al.* (1991), Philippot & Van Roermund (1992), and was observed during experimental deformation of polycrystalline diopside by Carter *et al.* (1972). The latter occurred at 1000–1200 °C with concomitant development of a clear CPO similar to those observed in naturally-deformed eclogites. Similar experiments by Boland & Tullis (1986) showed that deformation and grain boundary mobility are both promoted by addition of water.

The driving force for crystal growth and grain boundary mobility in aggregates (Urai *et al.*, 1986, Shimizu 1992) can be expressed as:

$$\Delta\mu = -\Delta(\sigma_n V) + \Delta f^{\text{chem}} + \Delta f^{\text{surf}} + \Delta f^{\text{elas}} + \Delta f^{\text{plas}}, \quad (2)$$

where $\Delta\mu$ is the difference of chemical potential for growth between the dissolving and growing interfaces, σ_n is the stress normal to these interfaces and V is the molar volume. The other terms refer to differences between grains with respect to chemical energy (Δf^{chem}), grain boundary energy (Δf^{surf}), elastic strain energy (Δf^{elas}) and plastic strain energy (Δf^{plas}). Δf^{surf} is usually neglected. If the two adjacent grains have the same composition, Δf^{chem} is null. ΔV and Δf^{elas} are very low also but not completely null if the two anisotropic crystals have different lattice orientations in an anisotropic stress field. This could favour growth of grains whose main compressible axis is close to the main stress direction (Kamb 1959, Hartman & Den Tex 1964, Paterson 1973). In the past, Helmstaedt *et al.* (1972) and Engels (1972) suggested the importance of this hypothetical driving force on omphacite. Due to the monoclinic symmetry, the main compressible axis of cpx and omphacite lies in the (010) plane at about 50° from [001] (Kumazawa 1969, Levien *et al.*, 1979, Bhagat *et al.*, 1992), and we can predict that such an effect would favour a [001] concentration at about 50° from the normal to S, a CPO which has never been observed. Thus, we can assume that V is constant and Δf^{elas} is negligible. Consequently, equation (2) is reduced to:

$$\Delta\mu = -V\Delta\sigma_n + \Delta f^{\text{plas}}. \quad (3)$$

Deformation-induced grain growth can operate in rocks through two types of mechanism: mass transfer processes and grain boundary migration (GBM). In the case of GBM, atoms for grain growth are supplied by adjacent crystals. $\Delta\sigma_n$ is null because σ_n is the same for both sides of the migrating grain boundary and difference in defect density between adjacent crystals (Δf^{plas}) is the only important driving force. On the other hand, when mass transfer processes operate, atoms for grain growth are mainly supplied by far-off grain dissolution and precipitate after inter or intra-crystalline transport. The first term of equation (3) is then also important because σ_n varies according to the interface orientation. Thus, crystals grow at faces under tension (σ_n low), while they dissolve at faces under compression (σ_n high).

When there is evidence for deformation-induced cpx growth, authors usually argue in favour of GBM operating during migration dynamic recrystallization (Carter *et al.*, 1972, Champness *et al.*, 1974, Kirby & Kronenberg 1984, Mercier 1985, Boland & Tullis 1986, Buatier *et al.*, 1991): Cpx strain-free neoblasts grow by GBM at the expense of strained paleoblasts and are in turn strained by dislocation creep. This mechanism is very well known in metallurgy and has been demonstrated in quartzites, marbles and peridotites (e.g. Urai *et al.*, 1986). It may have occurred in some of our samples in which variations in dislocation densities have been observed.

It is often assumed, on the other hand, that mass transfer processes are of secondary importance deep in the lithosphere, as they are swamped by dislocation creep at high T or high stress. Recent studies however tend to question this assumption (see discussion in Wheeler 1992). It should be emphasized that mass

transfer can play an important role in eclogites: Cracks within garnet filled with omphacite (Erambert & Austrheim 1993), overgrowth of strained omphacite crystals (Fig. 3b) or syntectonic omphacite veins (Hashimoto 1963, Essene & Fyfe 1967, Kazak 1968, Holland 1979, Carpenter 1980, Heinrich 1986, Philippot 1987, Philippot & Selverstone 1990, Philippot & Van Roermund 1992) provide strong evidence for diffusive mass transfer being active in eclogite facies, particularly in low-T fluid-rich eclogite conditions. Moreover, omphacite foliation wraps around garnets and forms typical 'pressure shadow' shapes (Fig. 3a), indicating that omphacite growth is sensitive to local changes in the stress orientation, a fact that can be explained by mass transfer but is difficult to explain by GBM (see above).

Grain boundary mobility, whatever the mechanism, modifies the shape but not the crystallographic orientation of a particular crystal. However, it may modify CPOs through selective growth of some grains and elimination of others. Strain-induced GBM rate varies in relation to the relative orientations of the two grains involved (Poirier & Guillopé 1979) and, in this way, may have an effect on CPOs but this effect cannot yet be estimated due to a lack of experimental calibrations. Alternatively, if mass transfer processes are operating, anisotropic growth/dissolution rate may also have an effect. This has been proposed by Etheridge *et al.* (1973) to explain the experimentally produced CPO in mica aggregates. The face growth/dissolution rates are proportional to the face attachment energies E_{att}. E_{att} in cpx increases in the following order: (010)<(100)≪(001) (Van Panhuys-Sigler & Hartman 1981). Therefore, crystals with [001] parallel to the tensional direction would grow faster than other grains, whereas crystals with [010] parallel to the compressional direction would dissolve more slowly. This would favour crystal orientations compatible with the observed omphacite CPOs. It can also explain the fabric of undeformed omphacite veins, in which crystals with [001] parallel to the tensional direction, i.e. perpendicular to the vein wall, develop preferentially (Philippot & Van Roermund 1992).

We can conclude that dislocation creep is testified by the presence of dislocations and well-ordered dislocation walls in omphacite. However, this mechanism alone cannot explain all the observed facts and other deformation mechanisms must be involved. These may include dynamic migration recrystallization by GBM and also mass transfer processes. Mechanical twinning and rotation recrystallization, on the other hand, have only played secondary roles.

DISCUSSION

One aim of this study was the characterization of omphacite microfabrics in relation to some of the deformation parameters (e.g. stress magnitude, strain rate and finite strain ellipsoid). Many studies have attempted to determine stress magnitudes during geological deformation, using 'paleo-piezometers' such as grain size, subgrain size and dislocation density. These techniques have mainly been used for olivine, quartz and calcite. In the case of cpx, Tullis (1980) proposed the use of twins to measure paleo-shear stress orientations. Avé Lallement (1978) calculated an empirical law at 1200°C to determine the flow stress from the neoblast size during dynamic migration recrystallization. Unfortunately, applying such piezometers to cpx is hampered by the lack of experimental verification and by the complexity of the deformation mechanisms. Finite strain ellipsoid also cannot be accurately quantified in the absence of primary markers. However, omphacite microfabric analysis allows a qualitative evaluation of the strain type (S to L-type) and intensity. Strong obliquities between omphacite [001] axis and L, visible in shear zones (Boundy *et al.*, 1992), suggest that CPOs might also be used to show evidence of simple shear.

A second aim was the identification of the mechanisms of deformation and fabric development, and this led to the conclusions of the previous section. These conclusions need to be verified by further experimental investigations. The rheology of omphacite, for example, is extrapolated from that of diopside and is not accurately known. The effect of mechanisms such as mass transfer and grain boundary migration need also to be investigated.

Although our understanding of omphacite rheology and behaviour during eclogite deformation is still limited, microfabric omphacite studies may have important applications.

A better knowledge of eclogite fabrics is useful to interpret seismic reflection data from deeper levels of subduction zones. Barruol & Mainprice (1993), for example, converted cpx fabrics into anisotropic seismic velocity data. However, it is already known that the seismic anisotropies of eclogites are less than 4%, even if a strong fabric exists (Kumazawa *et al.*, 1971, Babuska *et al.*, 1978, Barruol & Mainprice 1993, Fountain *et al.*, 1994). This is due to the cpx monoclinic symmetry which induces a dispersion of the linear compressibility ellipsoid.

It is known that eclogite or other high-P metamorphic rocks belong to various different geological terrains: thin- and thick-skinned continental crust; paleooceanic crust environment, etc. It is unknown if these different high P geological settings also correspond to different deformation types. In addition, during the past ten years, evidence for ultra-high P metamorphism, such as coesite and diamond in gneisses, garnet peridotites and eclogites, has been accumulated from various parts of the world (e.g. Chopin 1984, Smith 1984, Nixon *et al.*, 1986, Okay *et al.*, 1989, Sobolev & Shatsky 1990, Yang *et al.*, 1993). Understanding the mechanisms responsible for the transport of these rocks from an extreme depth to the surface is one of the major challenges in structural geology nowadays. Systematic eclogite fabric studies can play an important role in the solution of such questions in the future.

Acknowledgements—Support from CNRS (INSU, 'Programme DBT: les matériaux à haute pression') is gratefully acknowledged. TEM analyses were performed at the Laboratoire de Minéralogie Physique, Géosciences, Université de Rennes. P. Philippot allowed the publication of Fig. 3(b). P. Gillet, J. Ingrin, I. Ghose, M. Mendia, B. Reynard and C. Willaime are thanked for their help and discussions. J. Boland, D. Mainprice and Associate Editor R. Norris provided helpful comments. H.V.R. is grateful to Paris-7 University for a temporary research grant.

REFERENCES

Allmendinger, R. W. 1988. STEREONET; a plotting program for orientation data. Computer program + manual, 30 pp.

Ando, J. I., Fujino, K., Takeshita, T. 1993. Dislocation microstructures in naturally deformed silicate garnets. *Phys. Earth & Planet. Interiors* **80**, 105–116.

Ashworth, J. R. 1980. Deformation mechanisms in mildly shocked chondritic diopside. *Meteoritics* **15**, 105–115.

Ashworth, J. R. 1985. Transmission electron microscopy of L-group chondrites, 1. Natural shock effects. *Earth Planet. Sci. Lett.* **73**, 17–32.

Avé Lallement, H. G. 1967. Structures and petrofabric analysis of an 'Alpine-type' peridotite: the lherzolite of the French Pyrenees. *Leid. geol. Meded.* **42**, 1–27.

Avé Lallement, H. G. 1978. Deformation of diopside and websterite. *Tectonophysics* **48**, 1–27.

Babuska, V., Fiala, J., Mayson, D. J. & Liebermann, R. C. 1978. Elastic properties of eclogite rocks from the Bohemian Massif. *Cesk. Akad. Ved. Stud. Geophys. Geod.* **22**, 348–361.

Baker, D. W. & Carter, N. L. 1972. Seismic velocity anisotropy calculated for ultramafic minerals and aggregates. In: Flow and Fracture of Rocks (edited by Heard, H. C., Borg, I. Y., Carter, N. L. & Raleigh, C. B.). *Am. Geophys. Union, Geophysical Monograph* **16**, 157–166.

Barruol, G. & MainPrice, D. 1993. 3-D seismic velocities calculated from lattice-preferred orientation and reflectivity of a lower crustal section: examples of the Val Sesia section (Ivrea zone, northern Italy). *Geophys. J. Int.* **115**, 1169–1188.

Bell, P. M. & Davis, B. T. C. 1969. Melting relations in the system jadeite-diopside at 30 and 40 kilobars. *Am. J. Sci.* **267-A**, 17–32.

Bernard-Griffiths, J., Peucat, J. J., Cornichet, J., Ponce De Leon, I. & Gil Ibarguchi, J. I. 1985. U-Pb, Nd isotope and REE geochemistry in eclogites from Cabo Ortegal Complex, Galicia, Spain: an example of REE immobility conserving MORB-like patterns during high-grade metamorphism. *Chem. Geol.* **52**, 217–222.

Bhagat, S. S., Bass, J. D. & Smyth, J. R. 1992. Single-crystal elastic properties of omphacite-C2/c by Brillouin spectroscopy. *J. geophys. Res.* **B97**, 6843–6848.

Biggar, G. M. 1972. Diopside lithium metasilicate, and the 1968 temperature scale. *Mineralog. Mag.* **38**, 768–770.

Bingham, C. 1974. An antipodally symmetric distribution on the sphere. *Ann. Statist.* **2**, 1201–1225.

Binns, R. A. 1967. Barroisite-bearing eclogite from Naustdal, Sogn og Fjordane, Norway. *J. Petrol.* **8**, 349–371.

Boland, J. N. & Tullis, T. E. 1986. Deformation behavior of wet and dry clinopyroxenite in the brittle to ductile transition region. In: Mineral and Rock Deformation: Laboratory Studies (edited by Hobbs, B. E.). *Am. Geophys. Union, Geophysical Monograph* **36**, 35–49.

Boland, J. N. & Van Roermund, H. L. M. 1983. Mechanisms of exsolution in omphacites from high temperature, type B eclogites. *Phys. Chem. Minerals* **9**, 30–37.

Bouchardon, J. L. 1989. Témoins de cisaillements syn-éclogitisation; les éclogites blastomylonitiques à clastes d'omphacite du Levezou (Rouergue, Massif Central français). *C. r. hebd. Séanc. Acad. Sci., Paris (Série 2)* **309**, 69–72.

Bouchez, J. L. 1977. Plastic deformation of quartzites at low temperature in an area of natural strain gradient. *Tectonophysics* **39**, 25–50.

Boudier, F. 1978. Structure and petrology of the Lanzo peridotite massif (Piemont Alps). *Bull. geol. Soc. Am.* **89**, 1574–1591.

Boundy, T. M., Fountain, D. M. & Austreim, H. 1992. Structural arcs, western Norway: implications for deep crustal deformational processes. *J. Metamorphic Geol.* **10**, 127–146.

Buatier, M., Van Roermund, H. L. M., Drury, M. R. & Lardeaux, J. M. 1991. Deformation and recrystallisation mechanisms in naturally deformed omphacite from the Sesia–Lanzo zone. *Tectonophysics* **195**, 11–27.

Bunge, H. J. 1981. Fabric analysis by orientation distribution functions. *Tectonophysics* **78**, 1–21.

Bunge, H. J. 1985. Representation of preferred orientations. In: *Preferred Orientation in Deformed Metals and Rocks: An Introduction to Modern Texture Analysis* (edited by Wenk, H. R.). Academic Press, Inc., NY 73–108.

Carpenter, M. A. 1979. Contrasting properties and behaviour of antiphase domains in pyroxenes. *Phys. Chem. Minerals* **5**, 119–131.

Carpenter, M. A. 1980. Composition and cation order variations in sector-zoned blueschist pyroxene. *Am. Miner.* **65**, 313–320.

Carter, N. L., Baker, D. W. & Richard, P. G. 1972. Seismic anisotropy, flow and constitution of the upper mantle. In: Flow and Fracture of Rocks (edited by Heard, H. C., Borg, I. Y., Carter, N. L. & Raleigh, C. B.). *Am. Geophys. Union, Geophysical Monograph* **16**, 167–190.

Champness, P. E., Fyfe, W. S. & Lorimer, G. W. 1974. Dislocations and voids in pyroxene from low temperature eclogite: mechanism of eclogite formation. *Contr. Miner. Petrol.* **43**, 91–98.

Chopin, C. 1984. Coesite and pure pyrope in high grade blueschists of the Western Alps: A first record and some consequences. *Contr. Miner. Petrol.* **86**, 107–118.

Doukhan, J. C., Doukhan, N., Naze, L. & Van Duysen, J. C. 1985. Défauts de réseau et plasticité cristalline dans les pyroxènes; une revue. *Bull. Minéral.* **109**, 377–394.

Ellis, D. J. & Green, D. H. 1979. An experimental study of the effect of Ca upon garnet-clinopyroxene Fe-Mg exchange equilibria. *Contr. Miner. Petrol.* **71**, 13–22.

Engels, J. P. 1972. The catazonal poly-metamorphic rocks of Cabo Ortegal (NW Spain), a structural and petrographic study. *Leid. geol. Meded.* **48**, 83–133.

Erambert, M. & Austrheim, H. 1993. The effect of fluid and deformation on zoning and inclusion patterns in poly-metamorphic garnets. *Contr. Miner. Petrol.* **115**, 204–214.

Essene, E. J. & Fyfe, W. S. 1967. Omphacite in Californian metamorphic rocks. *Contr. Miner. Petrol.* **15**, 1–23.

Etchecopar, A. 1977. A plane kinematic model of progressive deformation in a polycrystalline aggregate. *Tectonophysics* **39**, 121–139.

Etchecopar, A. & Vasseur, G. 1987. A 3-D kinematic model of fabric development in polycrystalline aggregates: comparisons with experimental and natural examples. *J. Struct. Geol.* **9**, 705–717.

Etheridge, M. A., Paterson, M. S. & Hobbs, B. E. 1973. Experimentally produced preferred orientation in synthetic mica aggregates. *Contr. Miner. Petrol.* **44**, 275–294.

Fountain, D. M., Boundy, T. M., Austrheim, H. & Rey, P. 1994. Eclogite-facies shear zones, deep crustal reflectors? *Tectonophysics* **232**, 411–424.

Gil Ibarguchi, J. I., Mendia, M., Girardeau, J. & Peucat, J. J. 1990. Petrology of eclogites and clinopyroxene–garnet metabasites from the Cabo Ortegal Complex (north–western Spain). *Lithos* **25**, 133–162.

Gillet, P., Ingrin, J. & Chopin, C. 1984. Coesite in subducted continental crust. P-T history deduced from elastic model. *Earth Planet. Sci. Lett.* **70**, 426–436.

Godard, G. 1981. Lambeaux probables d'une Croûte Océanique Subductée: Les Éclogites de Vendée (Massif Armoricain, France). Thèse de 3ième cycle, Nantes, 153 pp.

Godard, G. 1988. Petrology of some eclogites in the Hercynides: the eclogites from the southern Armorican massif, France. In: Eclogites and Eclogite-Facies Rocks (edited by Smith, D. C.). *Developments in Petrology* **12**. Elsevier, Amsterdam, 451–519.

Griggs, D. T., Turner, F. J. & Heard, H. C. 1960. Deformation of rocks at 500 degrees to 800 degrees C., Chap. 4. In: Rock deformation (edited by Griggs, D. T.). *Mem. geol. Soc. Am.* **16**, 39–104.

Hartman, P. & Den Tex, E. 1964. Piezocrystalline fabrics of olivine in theory and nature. *Proc. XXII Int. Geol. Cong.* **section 4**, 84–114.

Hashimoto, M. 1963. Omphacite veins in metadiabase from Asahine in the Kantô Mountains, Japan. *Proc. Japan Acad.* **40**, 31–35.

Heinrich, C. A. 1986. Eclogite facies regional metamorphism of hydrous mafic rocks in the Central Alpine Adula Nappe. *J. Petrol.* **27**, 123–154.

Helmstaedt, H., Anderson, O. L. & Gavasci, A. T. 1972. Petrofabric studies of eclogite, spinel-websterite and spinel-lherzolith xenoliths from kimberlite-bearing breccia pipes in southeastern Utah and north–eastern Arizona. *J. geophys. Res.* **77**, 4350–4365.

Holland, T. J. B. 1979. High water activities in the generation of high pressure kyanite eclogites of the Tauern Window, Austria. *J. Geol.* **87**, 1–27.

Holland, T. J. B. 1990. Activities of components in omphacitic solid

solutions—an application of Landau theory to mixtures. *Contr. Miner. Petrol.* **105**, 446–453.

Hornemann, U. & Mueller, W. F. 1971. Shock-induced deformation twins in clinopyroxene. *Neues Jb. Miner. Mh.* **6**, 247–256.

Ingrin, J., Doukhan, N. & Doukhan, J. C. 1991. HT deformation of diopside single crystals. 2, TEM investigation of the induced defect microstructures. *J. geophys. Res.* **B96**, 14287–14297.

Ingrin, J., Doukhan, N. & Doukhan, J. C. 1992. Dislocation glide systems in diopside single crystals deformed at 800–900 °C. *Eur. J. Mineral.* **4**, 1291–1302.

Inoue, T. 1961. Structural-petrological studies of metamorphic complex of the Seburi Mountainland, with special reference to its bearing on the metamorphism of the Sangun metamorphic zone in Northern Kyûshû. *J. Sci. Hiroshima Univ.* **C-3**, 403–424.

Jakubith, M. & Seidel, P. 1982. Shock-loading experiments on eclogite. *Geophys. Res. Lett.* 408–411.

Ji, S., Salisbury, M. H. & Hanmer, S. 1993. Petrofabric P-wave anisotropy and seismic reflectivity of high-grade tectonites. *Tectonophysics* **222**, 195–226.

Kamb, W. B. 1959. Theory of preferred crystal orientation developed by crystallization under stress. *J. Geol.* **67**, 153–171.

Kappel, F. 1967. Die eklogite meidling im tal und mitterbachgraben im niederösterreichischen moldanubicum südlich der Donau. *Neues. Jb. Miner. Abh.* **107**, 266–298.

Kazak, A. P. 1968. Omphacite species from glaucophane schist, amphibolite and eclogite in the Southern Urals. *Doklady Acad. Sciences USSR, Earth Sci. Sections* **190**, 122–125.

Kirby, S. H. & Christie, J. M. 1977. Mechanical twinning in diopside Ca(Mg,Fe)Si2O6: structural mechanism and associated crystal defects. *Phys. Chem. Minerals* **1**, 137–163.

Kirby, S. H. & Kronenberg, A. K. 1984. Deformation of clinopyroxenite: evidence for a transition in flow mechanisms and semibrittle behavior. *J. geophys. Res.* **B-89**, 3177–3192.

Kojima, G. & Hide, K. 1957. On new occurrence of aegirine augite-amphibole-quartz-schists in the Sambagawa crystalline schists of the Besshi-Shirataki district, with special reference to the preferred orientation of aegirine, augite and amphibole. *J. Sci. Hiroshima Univ.* **C-2**, 1–20.

Kollé, J. J. & Blacic, J. D. 1982. Deformation of single-crystal clinopyroxenes. 1, Mechanical twinning in diopside and hedenbergite. *J. geophys. Res.* **B-87**, 4019–4034.

Kollé, J. J. & Blacic, J. D. 1983. Deformation of single-crystal clinopyroxenes. 2, Dislocation-controlled flow processes in hedenbergite. *J. geophys. Res.* **B-88**, 2381–2393.

Kozlowsky, K. 1965. Kompleks granulitowy Starego Gieraltowa w Gorach Zlotych. The granulitic complex of Stary Gieraltow—East Sudetes. *Archiwum Mineralogiczne* **25**, 5–123.

Kuijper, R. P., Vogel, D. E. & Den Tex, E. 1985. Eclogite–plagiopyrigarnite relations in the catazonal complexes of Northwest Spain. *Chem. Geol.* **50**, 163–171.

Kumazawa, M. 1969. The elastic constants of single-crystal orthopyroxene. *J. geophys. Res.* **74**, 5973–5980.

Kumazawa, M., Helmstaedt, H. & Masaki, K. 1971. Elastic properties of eclogite xenoliths from diatremes of the east Colorado Plateau and their implication to the mantle structure. *J. geophys. Res.* **76**, 1231–1247.

Levien, L., Weidner, D. J. & Prewitt, C. T. 1979. Elasticity of diopside. *Phys. Chem. Minerals* **4**, 105–113.

Litvin, Y. A. & Gasparik, T. 1993. Melting of jadeite to 16.5 GPa and melting relations on the enstatite-jadeite join. *Geochim. cosmochim. Acta* **57**, 2033–2040.

Lloyd, G. E. 1987. Atomic number and crystallographic contrast images with SEM: a review of back-scattered electron techniques. *Mineralog. Mag.* **51**, 3–19.

Lloyd, G. E., Law, R. D. & Schmid, S. M. 1987. A spherical electron channeling map for use in quartz petrofabric analysis: correction and verification. *J. Struct. Geol.* **9**, 251–254.

Lorimer, G. W., Champness, P. E. & Spooner, E. T. C. 1972. Dislocation distributions in naturally deformed omphacite and albite. *Nature Phys. Sci.* **239**, 108–109.

Mainprice, D. & Nicolas, A. 1989. Development of shape and lattice preferred orientations: applications to the seismic anisotropy of the lower crust. *J. Struct. Geol.* **11**, 175–189.

Mardia, K. V. 1972. *Statistics of Directional Data*. Academic Press, London/New York, 357 pp.

Mercier, J. C. 1985. Olivine and Pyroxenes. In: *Orientation in Deformed Metals and Rocks: An Introduction to Modern Texture Analysis* (edited by Wenk, H. R.). Academic Press Inc., NY 407–430.

Mockel, J. R. 1969. Structural petrology of the garnet-peridotite of Alpe Arami (Ticino, Switzerland). *Leid. geol. Meded.* **42**, 61–130.

Molinari, A., Canova, G. R. & Ahzi, S. 1987. A self-consistent approach of the large deformation polycrystal viscoplasticity. *Acta metall.* **35**, 2983–2994.

Mork, M. B. E., Kullerud, K. & Stable, A. 1988. Sm-Nd dating of Seve eclogites, Norbotten, Sweden. Evidence for early Caledonian (505 Ma) subduction. *Contr. Miner. Petrol.* **99**, 344–351.

Nicolas, A. & Poirier, J. P. 1976. *Crystalline Plasticity and Solid State Flow in Metamorphic Rocks*. John Wiley & Sons, NY, 444 pp.

Nixon, P. H., Davies, G. R., Slodkevitch, V. V. & Bergman, S. C. 1986. Graphite pseudomorphs after diamond in the eclogite-peridotite massif of Beni-Bousera, Morocco, and a review of anomalous diamond occurrences. *Fourth Int. Kimberlite Conf., Geol. Soc. Australia Abstr.* **16**, 412–414.

Okay, A. I., Xu, S. & Sengor, A. M. C. 1989. Coesite from the Dabie Shan eclogites, central China. *Eur. J. Mineral.* **1**, 595–598.

Paterson, M. S. 1973. Non-hydrostatic thermodynamics and its geological applications. *Rev. Geophys. & Space Phys.* **11**, 355–389.

Péquignot, G., Lardeaux, J. M. & Caron, J. M. 1984. Recristallisation d'éclogites de basse température dans les métabasaltes corses. *C. r. hebd. Séanc. Acad. Sci., Paris (Série 2)* **299**, 871–874.

Peucat, J. J., Vidal, P., Godard, G. & Postaire, B. 1982. Precambrian U-Pb zircon ages in eclogite and garnet-pyroxenites from south Brittany (France): an old oceanic crust in the West European Hercynian belt? *Earth Planet. Sci. Lett.* **60**, 70–78.

Philippot, P. 1987. 'Crack seal' vein geometry in eclogitic rocks. Formation de veines par fracturation incrémentale et remplissage progressif dans les conditions du métamorphisme éclogitique. *Geodinamica Acta* **1**, 171–181.

Philippot, P. & Selverstone, J. 1990. Trace-element-rich brines in eclogite veins: implications for fluid composition and transport during subduction. *Contr. Miner. Petrol.* **106**, 417–430.

Philippot, P. & Van Roermund, H. L. M. 1992. Deformation processes in eclogitic rocks: evidence for the rheological delamination of the oceanic crust in deeper levels of subduction zones. *J. Struct. Geol.* **14**, 1059–1077.

Poirier, J. P. & Guillopé, M. 1979. Deformation induced recrystallization of minerals. *Bull. Minéral.* **102**, 67–74.

Raleigh, C. B. & Talbot, J. L. 1967. Mechanical twinning in naturally and experimentally deformed diopside. *Am. J. Sci.* **265**, 151–165.

Raterron, P. & Jaoul, O. 1991. High-temperature deformation of diopside single crystal. 1, Mechanical data. *J. geophys. Res.* **B-96**, 14277–14286.

Raterron, P., Doukhan, N., Jaoul, O. & Doukhan, J. C. 1994. High temperature deformation of diopside IV: predominance of {110} glide above 1000°C. *Phys. Earth & Planet. Interiors* **82**, 209–222.

Rossi, G. 1988. A review of the crystal-chemistry of clinopyroxenes in eclogites and other high-pressure rocks. In: Eclogites and eclogite-facies rocks (edited by Smith, D. C.). *Developments in Petrology* **12**. 237–270.

Rummel, F. 1969. Studies of time-dependant deformation of some granite and eclogite rock samples under uniaxial, constant compressive stress and temperatures up to 400 °C. *Zeitschr. Geophysik* **35**, 17–42.

Ryabinin, Y. N., Beresnev, B. I., Martynov, Y. D. & Prishchepov, V. F. 1973. Influence of pressure upon the deformation-dependent properties of rocks. *Phys. Solid Earth* (English Edn.) **4**, 233–236.

Shimizu, I. 1992. Non-hydrostatic and non-equilibrium thermodynamics of deformable materials. *J. geophys. Res.* **B-97**, 4587–4597.

Siegesmund, S., Takeshita, T. & Kern, H. 1989. Anisotropy of Vp and Vs in an amphibolite of the deeper crust and its relationship to the mineralogical, microstructural and textural characteristics of the rocks. *Tectonophysics* **157**, 25–38.

Skrotzki, W. 1994. Defect structure and deformation mechanisms in naturally deformed augite and enstatite. *Tectonophysics* **229**, 43–68.

Smith, B. K. & Wenk, H. R. 1980. Dislocations in deformed garnet: applications in eclogite-derived pyralspite. *Eos.* **61**, 375.

Smith, D. C. 1984. Coesite in clinopyroxene in the Caledonides and its implications for geodynamics. *Nature, Lond.* **310**, 641–644.

Sobolev, N. V. & Shatsky, V. S. 1990. Diamond inclusions in garnets from metamorphic rocks: a new environment for diamond formation. *Nature, Lond.* **343**, 746.

Tullis, T. E. 1980. The use of mechanical twinning in minerals as a measure of shear stress magnitudes. *J. geophys. Res.* **B-85**, 6263–6268.

Urai, J. L., Means, W. D. & Lister, G. S. 1986. Dynamic recrystallisa-

tion of minerals. In: Mineral and Rock Deformation: Laboratory Studies (edited by Hobbs, B. E.). *Am. Geophys. Union. Geophysical Monograph* **36**, 161–199.

Van Der Molen & Van Roermund, H. 1986. The pressure path of solid inclusions in minerals: the retention of coesite inclusions during uplift. *Lithos* **19**, 317–324.

Van Duysen, J. C. & Doukhan, J. C. 1984. Room temperature microplasticity of a spodumene LiAlSi2O6. *Phys. Chem. Minerals* **10**, 125–132.

Van Panhuys-Sigler, M. & Hartman, P. 1981. Morphologie théorique de certains pyroxènes déduite de la structure cristalline. *Bull. Minéral.* **104**, 95–106.

Van Roermund, H. L. M. 1983. Petrofabrics and microstructures of omphacites in a high temperature eclogite from the Swedish Caledonides. *Bull. Minéral.* **106**, 709–713.

Van Roermund, H. L. M. 1984. Omphacite microstructures from a Spanish eclogite. *Textures and Microstructures* **6**, 105–116.

Van Roermund, H. L. M. 1985. Eclogites of the Seve Nappe, central Scandinavian Caledonides. In: *The Caledonide Orogen. Scandinavia and Related Areas* (edited by Gee, D. G. & Sturt, B. A.). John Wiley & Sons, NY, 873–886.

Van Roermund, H. L. M. 1989. High-pressure ultramafic rocks from the Allochthonous Nappes of the Swedish Caledonides. In: *The Caledonide Geology of Scandinavia* (edited by Gayer, R.). Graham and Trotman, 205–219.

Van Roermund, H. L. M. 1992. Thermal and deformation induced omphacite microstructures from eclogites. Implications for the formation and uplift of HP metamorphic terrains In: *Recent Trends in Mineralogy* (edited by Int. Research Council). 117–151.

Van Roermund, H. L. M. & Bakker, E. 1984. Structure and metamorphism of the Tangen-Inviken area, Seve Nappe, Central Scandinavian Caledonides. *Geol. För. Stockh. Förh.* **105**, 301–319.

Van Roermund, H. L. M. & Boland, J. N. 1981. The dislocation substructures of naturally deformed omphacites. *Tectonophysics* **78**, 403–418.

Van Roermund, H. L. M. & Lardeaux, J. M. 1991. Modification of antiphase domain sizes in omphacite by dislocation glide and creep mechanisms and its petrological consequences. *Mineralog. Mag.* **55**, 397–407.

Van Zuuren, A. 1969. Structural petrology of an area near Santiago de Compostela (NW Spain). *Leid. geol. Meded.* **45**, 1–71.

Vogel, D. E. 1967. Petrology of an eclogite- and pyrigarnite-bearing polymetamorphic rock complex at Cabo Ortegal, NW Spain. *Leid. geol. Meded.* **40**, 121–213.

Von Herrmann, A., Paulitsch, P. & Roch, C. 1979. Steirische Gefuege (Oesterreich). *Mitteilungsblatt—Abteilung für Mineralogie am Landesmuseum Joanneum* **D15, S104**, 19–26.

Von Mises, R. 1928. Mechanik der plastichen Formanderung von kristallen. *Z. Angew. Math. Mech.* **8**, 161–185.

Wenk, H. R. & Christie, J. M. 1991. Comments on the interpretation of deformation textures in rocks. *J. Struct. Geol.* **13**, 1091–1110.

Wenk, H. R. & Wilde, W. R. 1972. Orientation distribution for three Yule marble fabrics. In: Flow and Fracture of Rocks (edited by Heard, H. C., Borg, I. Y., Carter, N. L. & Raleigh, C. B.). *Am. Geophys. Union, Geophysical Monograph* **16**, 83–94.

Wheeler, J. 1992. Importance of pressure solution and Coble creep in the deformation of polymineralic rocks. *J. geophys. Res.* **B-97**, 4579–4586.

Williams, D. W. & Kennedy, G. C. 1970. The melting of jadeite to 60 kilobars. *Am. J. Sci.* **269**, 481–488.

Wilson, C. J. L. 1986. Deformation induced recrystallisation of ice: the application of in-situ experiments. In: Mineral and Rock Deformation: Laboratory Studies (edited by Hobbs, B. E.). *Am. Geophys. Union, Geophysical Monograph* **36**, 213–232.

Yang, J., Godard, G., Kienast, J. R., Lu, Y. & Sun, J. 1993. Ultrahigh-Pressure (60 Kbar) magnesite-bearing garnet peridotites from Northeastern Jiangsu, China. *J. Geol.* **101**, 541–554.

Yoder, H. S. 1952. Change of melting point of diopside with pressure. *J. Geol.* **60**, 364–374.

Yoshino, G. 1961. Structural-petrological studies of peridotite and associated rocks of the Higashi-Akaishi-Yama district, Shikoku, Japan. *J. Sci. Hiroshima Univ.* **C-3**, 343–402.

Yoshino, G. 1964. Ultrabasic mass in the Higashiakaishiyama district, Shikoku, Southwest Japan. *J. Sci. Hiroshima Univ.* **C-4**, 333–364.